AD-A054 786 AERONAUTICAL RESEARCH ASSOCIATES OF PRINCETON INC N J F/G 11/4
A NEW FINITE ELEMENT TECHNIQUE AND A STUDY OF RESIDUAL STRESS I--ETC(U)
APR 78 T B MCDONOUGH F44620-76-C-0122
UNCLASSIFIED ARAP-336 AFOSR-TR-78-0957 NL

| OF |
AD
A054786

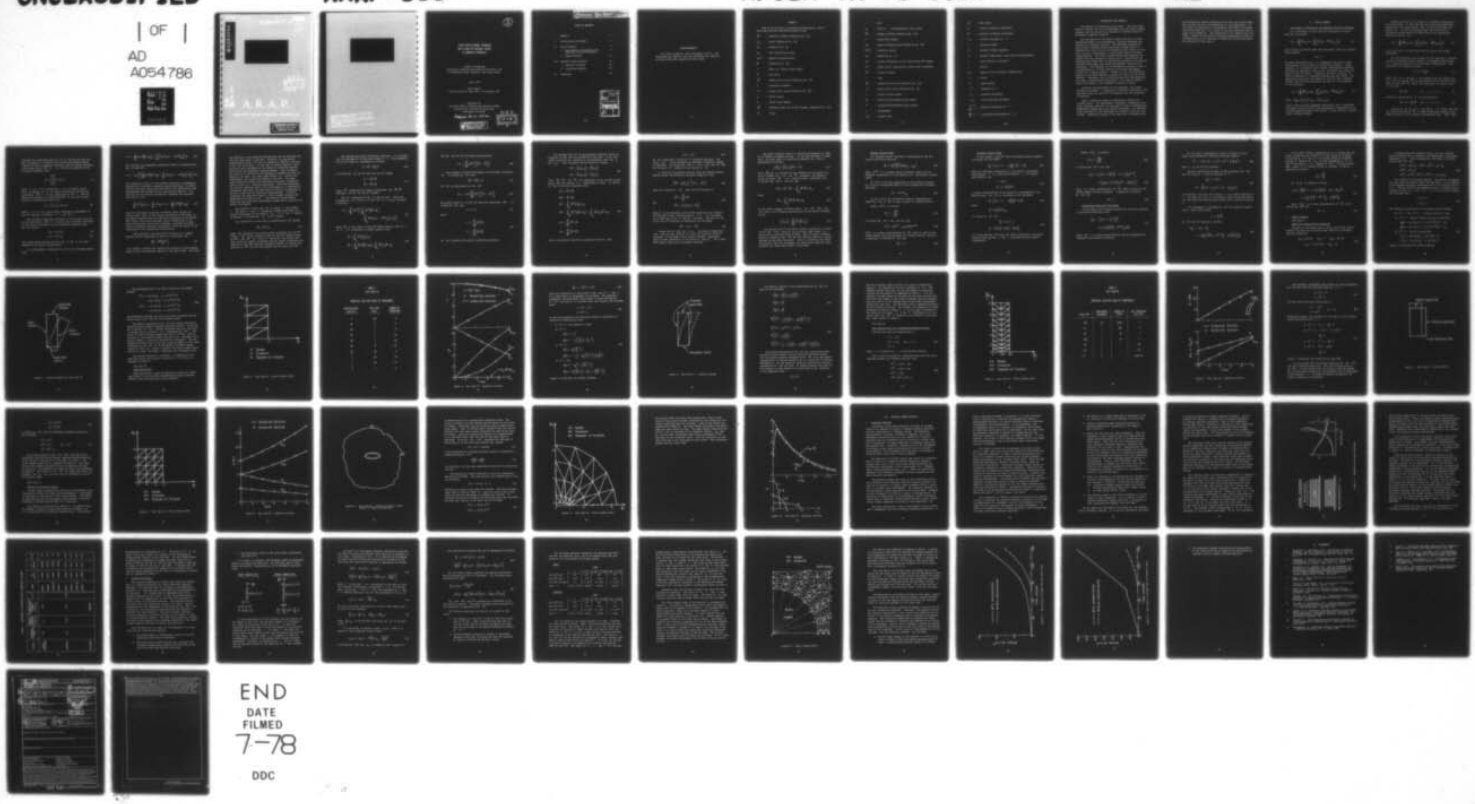

END
DATE
FILMED
7-78
DDC

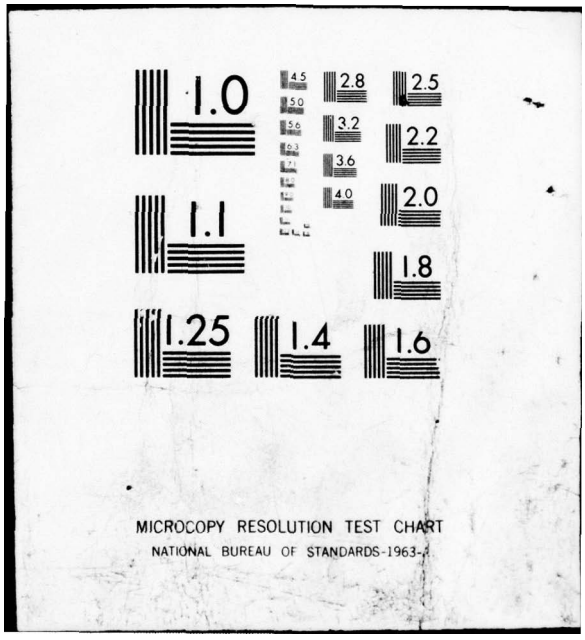
1.0
1.1
1.25
1.4
1.6
1.8
2.0
2.2
2.5
2.8
3.2
3.6
4.0
4.5
5.0
5.6
6.3
MICROCOPY RESOLUTION TEST CHART
NATIONAL BUREAU OF STANDARDS-1963-A

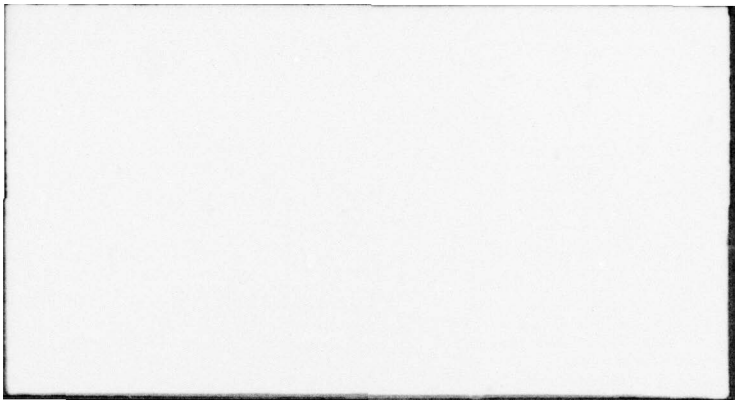

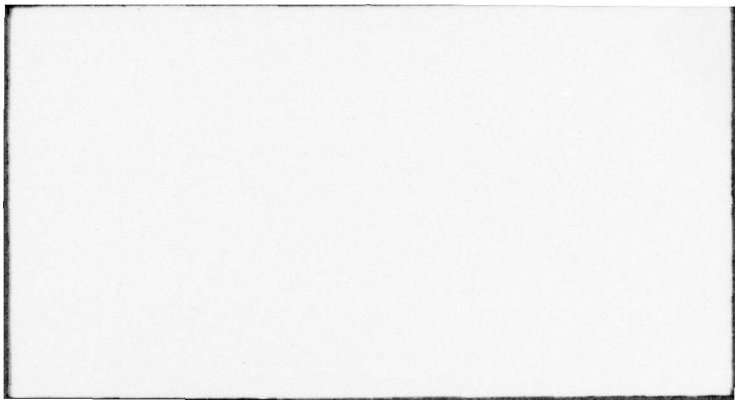

(2)

A NEW FINITE ELEMENT TECHNIQUE AND A STUDY OF RESIDUAL STRESS IN COMPOSITE MATERIALS

Thomas B. McDonough
Aeronautical Research Associates of Princeton, Inc.
50 Washington Road, Princeton, New Jersey 08540

April 1978

Final Report
For the Period 15 June 1976 - 30 November 1977

Prepared for
Air Force Office of Scientific Research (AFSC)
Building 410, Bolling Air Force Base
Washington, DC 20332

F44620-76-C-0122

TABLE OF CONTENTS

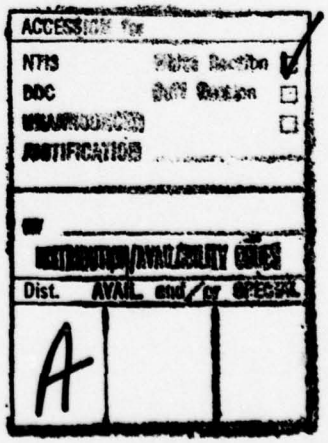

ACKNOWLEDGEMENT

The author thanks Mr. Ross Contiliano, A.R.A.P., for developing the computer codes and performing the numerical solutions which were required for this study.

SYMBOLS

Some of the notation is borrowed from References 1 and 2, where more detailed descriptions may be found.

$\overset{m}{[A]}$ ~ material stiffness defined by Eq. (31)

A_{ij} ~ tensor defined by Eq. (79)

[B] ~ defined by Eq. (8)

B_{ij} ~ left Cauchy-Green tensor

D-O-P ~ degree-of-polymerization

e^{mi} ~ defined by Eq. (16)

E ~ Green - St. Venant strain tensor

f^k ~ body force

$\overset{m}{\{f\}}$ ~ element force vector defined by Eq. (19)

F ~ deformation gradient

{F} ~ global force vector defined by Eq. (24)

g ~ metric tensor

G ~ scaler shear modulus

$\overset{m}{[G]}$ ~ incidence array for the m^{th} element, defined by Eq. (15)

I_B $\quad tr\, B_{ij}$

J ~ Det F

J_N ~ value of J corresponding to zero stress

$[\overset{m}{k}]$ ~ element stiffness defined by Eq. (33)

K ~ scaler bulk modulus

$[K]$ ~ global stiffness matrix defined by Eq. (34)

$K^{\alpha\gamma\beta\delta}$ ~ elasticity tensor

$[N]$ ~ defined by Eq. (7)

$\{q\}$ ~ current coordinates of the nodes of the m^{th} element

$\{Q\}$ ~ global vector representing current node coordinates

S^k ~ surface traction

t ~ time

$\{\overset{m}{t}\}$ ~ element force vector defined by Eq. (19)

$\{T\}$ ~ global force vector defined by Eq. (24)

T ~ Cauchy's stress tensor

T_R ~ first Piola-Kirchhoff stress tensor

$\tilde{T}$ ~ second Piola-Kirchhoff stress tensor

u ~ displacement

V.W. ~ virtual work

$w_i{}^j$ ~ spin tensor

z^i ~ current coordinate (Cartesian)

Z^K ~ material coordinate (Cartesian)

$\Delta( )$ ~ a finite increment of ( )

δ ~ variation symbol

ε^T ~ uniaxial thermal expansion

ε^P ~ uniaxial dimensional strain due to polymerization

μ ~ shear modulus or viscosity

ρ ~ density

ρ_R ~ density of the reference configuration

{ } ~ vector

[ ] ~ square matrix

$[\ ]^T$ ~ transpose of [ ]

$( )_{,i}$ ~ covariant derivative

$( )_{;K}$ ~ total covariant derivative

$(\dot{}\,)$ or $\frac{d}{dt}( )$ ~ material derivative of ( )

$\frac{dr}{dt}( )$ ~ corotational derivative of ( ).

I. INTRODUCTION AND SUMMARY

Two studies are presented in this report. The first (presented in Section II) is the development of a new finite element solution, and the second is an analysis of residual stress in filamentary composite material.

The new feature of the finite element solution is in the formulation phase of the development; existing procedures are used for the numerical solution. The technique presented is restricted to problems usually described as quasi-static or creeping flow, but it is not restricted by small strain or rotation, nor is it specialized to a particular theory of constitutive behavior. The finite element equilibrium equations are derived from the principle of virtual work — specifically the representation which uses the deformation gradient as the measure-of-strain which makes this technique different from existing techniques. One advantage of the deformation gradient is that it is expressible as a linear function of the node coordinates exactly for a simplex element. Another is that the deformation gradient is an adept measure-of-strain for both solid and fluid behavior. Therefore, the new technique may offer advantages for the study of solid-fluid interactions or for material behavior which fits neither of the concepts of solids or fluids.

Following the development of the technique, four sample problems are studied. A comparison of numerical predictions with some exact analytic solutions is presented, and the comparison is excellent.

Quite a different subject is addressed in Section III: residual stress. Its development in polymeric filamentary reinforced composite materials is discussed in terms of differential dimensional changes that occur during processing. Two phenomena which contribute to the development of residual stress are considered: dimensional change of the resin due to polymerization

and differential thermal expansion of the resin and reinforcement upon cooling from the cure temperature to room temperature. In the theory of composites in use presently the effects of polymerization are neglected; it's a goal of the study presented here to assess this assumption. This assumption is not supported by this study — neither on the basis of available experimental studies of residual stress nor on the basis of numerical calculations which are presented in this report.

II. FINITE ELEMENT

1. Development of Formulation and Numerical Solution Technique

It is convenient to start with the definition of Virtual Work for a continuum[1]:

$$V.W. = \oint_S S^k \delta z_k \, da + \int_v \left[\rho f^k \delta z_k - T^{km} \delta z_{k,m} \right] dv \qquad (1)$$

The Principle of Virtual Work (for quasistatic motion or creeping flow) requires

$$V.W = 0$$

The form represented by Eq. (1) encompasses arbitrarily large displacements and all models of constitutive behavior. Unfortunately, it is referred to the current configuration (Eulerian description) completely, which is not convenient for solids, but which is used for fluids. Generally, one uses a form of V.W. which is referred to a reference configuration for solids. The appropriate quantities are defined in terms of their transformations from the above quantities and then Eq. (1) transforms to the following:

$$V.W. = \oint_S T_R^{NK} \delta u_N \, da_K + \int_V \left[\rho_R f^N \delta u_N - \tilde{T}^{NM} \delta E_{NM} \right] dV \qquad (2)$$

where $\delta E_{NM} \equiv \frac{1}{2} \left(\delta z^k_{;N} \, z_{k;m} + z^k_{;N} \, \delta z_{k;m} \right)$

This is the so-called Lagrangian description, and it represents a logical starting place for the development of generally all of the published developments for solids, at least for the so-called direct stiffness models.

Another form for V.W. in terms of a reference configuration can be developed. In this case the first Piola-Kirchhoff representation of the stress tensor (T_R) is used rather than the second $(\tilde{T})$. As for the previous form, the third form is developed by substituting the definitions of the appropriate quantities into Eq. (1):

$$V.W. = \oint_S T_R^{kK} \delta z_k \, dA_K + \int_V \left[\rho_R f^k \delta z_k - T_R^{kM} \delta z_{k;M} \right] dV \qquad (3)$$

It is this form of virtual work which is used in the present development.

Now the kinematics of an element will be described. Consider a single tetrahedral element subject to homogeneous deformation (i.e., measured relative to the reference configuration). This deformation is defined as follows:

$$z^i = e^i + F_K^i Z^K \qquad (4)$$

where the e^i's and F_K^i's are constant over the element volume. The coordinates $\overset{n}{q}{}^i$ are identified with the current coordinates of each node $\overset{n}{z}{}^i$ where the superindex "n" refers to one of the nodes:

$$\overset{n}{q}{}^i \equiv \overset{n}{z}{}^i \qquad \text{for } n = 1, 2, 3, 4 \qquad (5)$$

Therefore, evaluating Eq. (4) at the nodes gives

$$\overset{n}{q}{}^i = e^i + F_K^i \overset{n}{Z}{}^K \qquad \text{for } n = 1, 2, 3, 4 \qquad (6)$$

Solving Eq. (6) for e^i's and F_K^i's, it follows that they are linear functions of $\overset{n}{q}{}^i$'s whose coefficients depend on the nodal positions in the reference configuration only. After these

solutions are substituted into Eq. (4), it follows that the current coordinate of a material point within the element depends linearly on both its material coordinate and the current positions of the nodal points $\left({}^{n}q^{i}\text{'s}\right)$. Eq. (4) may be presented in the following convenient form:

$$\{z\} \equiv \begin{Bmatrix} z^1 \\ z^2 \\ z^3 \end{Bmatrix} = [N]\{q\} \tag{7}$$

where N is a 3×12 matrix and q is a 12-element vector. Also, the elements of N are linear functions of the material coordinates $(Z^K\text{'s})$ and are independent of ${}^{n}q^{i}\text{'s}$. Now the deformation gradient is computed from Eq. (7) and can be represented in the following matrix form:

$$\{F\} \equiv \left\{z^i{}_{;K}\right\} = [B]\{q\} \tag{8}$$

where B is a 9×12 matrix whose elements are independent of both the material coordinates $Z^i\text{'s}$ and ${}^{n}q^{i}\text{'s}$.

Now consider an arbitrary variation of the current positions of the nodal points $\left({}^{n}q^{i}\text{'s}\right)$ and derive the associated variations of the current coordinates and the deformation gradient from Eqs. (7) and (8):

$$\{\delta z\} = [N]\{\delta q\} \tag{9}$$

$$\{\delta F\} = [B]\{\delta q\} \tag{10}$$

This simple result follows the fact that N and B are independent of the current configuration.

It is convenient to represent Eq. (3) in the following matrix form:

$$V.W. = \oint_S \{\delta z\}^T \left\{ T_R^{kK} \, dA_K \right\} + \int_V \left[\{\delta z\}^T \rho_R \{f\} - \{\delta F\}^T \left\{ T_R \right\} \right] dV \qquad (11)$$

Now introduce the homogeneous deformation which is represented by Eqs. (9) and (10):

$$V.W. = \{\delta q\}^T \left[\left[\oint_S [N]^T \left\{ T_R^{kK} \, dA_K \right\} + \int_V [N]^T \rho_R \{f\} - [B]^T \left\{ T_R \right\} dV \right] \right] \qquad (12)$$

This formula for the V.W. of an element subjected to homogeneous deformation is otherwise completely general and exact; no approximations have been introduced which would limit arbitrarily large displacements and strains and the constitutive behavior. V.W. must be zero for arbitrary variations, therefore the bracketed term must be zero.

$$\int_V [B]^T \left\{ T_R \right\} dV = \int_V [N]^T \rho_R \{f\} \, dV + \oint_S [N]^T \left\{ T_R^{kK} \, dA_K \right\} \qquad (13)$$

Once the constitutive equation is defined, which relates the stress tensor $\left(T_R\right)$ to the current coordinates of the nodes (q), the above equation yields the equilibrium equation for an element. Fortunately, there have been many recent contributions to the field of nonlinear constitutive equations, including the formulation of general invariance requirements, which are useful in the development of the formulation required here.

Very generally, the constitutive equation for a simple material may be represented in terms of a functional (H) [2]:

$$T_R^{kM} = H^{kM} \left[F_N^i(t) \right] \qquad (14)$$

It is useful to discuss the constitutive equation in these general terms so that the discussion applies to any ideal model. Of course,

the specifics of the equations sketched here can be developed only after an ideal model is selected. Generally, an approximate representation of Eq. (14) will be required to develop a solution to Eq. (13) iteratively. In the case of elastic behavior "exact" solutions can be developed by the method of successive approximations even for moderately large increments. This is because the stress is a function of the deformation gradient and does not depend on the path. For other ideal models, e.g., plastic and viscoelastic, the stress does depend on the path. For these cases numerical solutions are developed using small incremental steps in time (i.e., marching techniques). With this background the solution technique used in this development is a combination; incremental time steps are taken and the solution is developed at the end of each step by successive approximations. Iterative techniques that have been used for finite element solutions are described by Stricklin et al.[3]. The modified Newton-Raphson method has been used with considerable success and is used for the present development.

Now consider a finite body (B) of volume V and surface S. Partition B into m tetrahedral elements and denote the current coordinates of the nodes by $\{Q\}$. If B has N degrees-of-freedom, it follows that $\{Q\}$ is an N-vector.

The connectivity of the model is established by the mapping

$$\{\overset{m}{q}\} = [\overset{m}{G}]\{Q\} \tag{15}$$

where $\{\overset{m}{q}\}$ represents the current nodal coordinates for the m^{th} element, $[\overset{m}{G}]$ is the incidence array for the m^{th} element defined by Oden[4], and $[\overset{m}{G}]$ is a six by N matrix for the present case. Also, since the element coordinates and the global coordinates are referred to the same Cartesian coordinate system, it follows that each row of $[\overset{m}{G}]$ has one unit element and the others are zero.

Now consider the global equilibrium equations. It's assumed that the deformation is piece-wise linear on B. The deformation of the m^{th} element is represented as follows:

$$z^i = \overset{m}{e}{}^i + \overset{m}{F}{}^i_K \, Z^K \tag{16}$$

It follows Eqs. (7) and (8) that for the m^{th} element

$$\begin{aligned} \{z\} &= [\overset{m}{N}]\,\{\overset{m}{q}\} \\ \{\overset{m}{F}\} &= [\overset{m}{B}]\,\{\overset{m}{q}\} \end{aligned} \tag{17}$$

where $\{\overset{m}{q}\}$ represents the current coordinates, and $[\overset{m}{N}],[\overset{m}{B}]$ represent $[N],[B]$ for the m^{th} element.

The V.W. represented by Eq. (3) must be zero. After substituting Eq. (17) into Eq. (3) the V.W. of B may be expressed as follows:

$$\text{V.W.} = \sum_{m=1}^{M} \{\delta\overset{m}{q}\}^T \left[\left[\int_{S^*_m} [\overset{m}{N}]^T \left\{ T_R^{kK} \, dA_K \right\} + \int_{V_m} [\overset{m}{N}]^T \rho_R \{f\} - [\overset{m}{B}]^T \left\{ T_R \right\} dV_m \right] \right] \tag{18}$$

where S^*_m is the surface of the m^{th} element which is part cf S of B. It's convenient to define element forces:

$$\begin{aligned} \{\overset{m}{t}\} &\equiv \int_{V_m} [\overset{m}{B}]^T \left\{ T_R \right\} dV_m \\ \{\overset{m}{f}\} &\equiv \int_{S^*_m} [\overset{m}{N}]^T \left\{ T_R^{kK} \, dA_K \right\} + \int_{V_m} [\overset{m}{N}]^T \rho_R \{\overset{m}{f}\} \, dV_m \end{aligned} \tag{19}$$

Then Eq. (18) has the following representation:

$$V.W. = \sum_{m=1}^{M} \{\delta \overset{m}{q}\}^T \left[\left[\{\overset{m}{f}\} - \{\overset{m}{t}\} \right] \right] \tag{20}$$

Now consider a virtual displacement of the global coordinates $\{Q\}$. It follows Eq. (15) that

$$\{\delta \overset{m}{q}\} = [\overset{m}{G}] \{\delta Q\} \tag{21}$$

Eq. (21) is substituted into Eq. (20).

$$V.W. = \{\delta Q\}^T \sum_{m=1}^{M} [\overset{m}{G}]^T \left[\left[\{\overset{m}{f}\} - \{\overset{m}{t}\} \right] \right] \tag{22}$$

Now require that V.W. be zero for arbitrary variations $\{\delta Q\}$, it follows Eq. (22) that

$$\{T\} = \{F\} \tag{23}$$

where

$$\begin{aligned} \{T\} &\equiv \sum_{m=1}^{M} [\overset{m}{G}]^T \{\overset{m}{t}\} \\ \{F\} &\equiv \sum_{m=1}^{M} [\overset{m}{G}]^T \{\overset{m}{f}\} \end{aligned} \tag{24}$$

Eq. (23) represents the global equilibrium equations.

For creeping flow all of the preceding equations, which are functions of time, must be satisfied for any time. If the individual quantities are evaluated at two different times, say t_n and t_{n+1}, then increments may be defined as follows:

$$\{\Delta \overset{m}{q}\} \equiv \left\{\overset{m}{q}\left(t_{n+1}\right)\right\} - \left\{\overset{m}{q}\left(t_n\right)\right\}$$
$$\{\Delta Q\} \equiv \left\{Q\left(t_{n+1}\right)\right\} - \left\{Q\left(t_n\right)\right\} \tag{25}$$

Since $[\overset{m}{N}]$, $[\overset{m}{B}]$, and $[\overset{m}{G}]$ are independent of the current coordinates, they are constant (i.e., independent of time). It follows Eq. (25) and previous equations that

$$\{\Delta z\} = [\overset{m}{N}]\{\Delta \overset{m}{q}\}$$

$$\{\Delta \overset{m}{F}\} = [\overset{m}{B}]\{\Delta \overset{m}{q}\}$$

$$\{\Delta \overset{m}{t}\} = \int_{V_m} [\overset{m}{B}]^T \left\{\Delta T_R\right\} dV_m$$

$$\{\Delta \overset{m}{f}\} = \int_{S_m^*} [\overset{m}{N}]^T \left\{\Delta T_R^{kK}\, dA_K\right\} + \int_{V_m} [\overset{m}{N}]^T \rho_R \{\Delta \overset{m}{f}\}\, dV_m \tag{26}$$

$$\{\Delta T\} = \sum_{m=1}^{M} [\overset{m}{G}]^T \{\Delta \overset{m}{t}\}$$

$$\{\Delta F\} \quad \sum_{m=1}^{M} [\overset{m}{G}]^T \{\Delta \overset{m}{f}\} \quad ,$$

and the incremental equilibrium equations follow Eq. (23).

$$\{\Delta T\} = \{\Delta F\} \tag{27}$$

Eq. (27) represents a system of N nonlinear equations. The vector $\{\Delta F\}$, which represents an increment of applied loading, is specified. It follows Eqs. (26)[3,5], (17)[2], (15), and (14) that the N-vector $\{\Delta T\}$ depends on the history of $\{Q\}$.

To solve the incremental solution using the modified Newton-Raphson method the following recurrence formula is used.

$$\{\overset{r+1}{\Delta Q}\} = \left[K\left(t_1\right)\right]^{-1}\left\{\{\Delta F\} - \{\overset{r}{\Delta T}\}\right\} \tag{28}$$

where the estimate of $\{\Delta Q\}$ after the r^{th} iteration is

$$\{\overset{R}{\Delta Q}\} \equiv \sum_{r=1}^{R} \{\overset{r}{\Delta Q}\} \tag{29}$$

and

$$\{\overset{R}{\Delta T}\} \equiv \left\{\Delta T\left(Q\left(t_1\right) + \overset{R}{\Delta Q}\right)\right\}$$

$\left[K\left(t_1\right)\right]$ is an invertible matrix which represents the stiffness of the global finite element model at $t = t_1$. For the moment we'll leave the choice of $\left[K\left(t_1\right)\right]$ arbitrary. The error at the end of the r^{th} iteration is measured by the following:

$$\{\overset{R}{e}\} \equiv \{\Delta F\} - \{\overset{R}{\Delta T}\} \tag{30}$$

Assume that Eq. (27), for $t = t_1$, possesses a unique solution. Then for any $\left[K\left(t_1\right)\right]$ for which the iterative solution converges, it converges to the correct solution. Apparently, there is some flexibility in the choice of $\left[K\left(t_1\right)\right]$, for a given ideal model, which gives convergent solutions.

The global stiffness matrix is selected conveniently in terms of the element stiffness matrices. If the time increment is taken short, the ideal model of constitutive behavior [Eq. (14)] is approximated as follows:

$$\left\{\Delta \overset{m}{T}_R\right\} = \left[\overset{m}{A}\left(t_1\right)\right]\{\Delta \overset{m}{F}\} + \{\overset{m}{\tau}\} \tag{31}$$

where $\left[\overset{m}{A}\left(t_1\right)\right]$ is a measure of the stiffness of the material in the m^{th} element for $t = t_1$ and $\{\overset{m}{\tau}\}$ represents the change in stress for fixed $\{\overset{m}{F}\}$, e.g., thermal stress, relaxation, etc. It follows Eqs. $(26)^{2,3}$ and (31) that

$$\{\Delta \overset{m}{t}\} = [\overset{m}{k}]\ \{\Delta \overset{m}{q}\} + \int_{V_m} [\overset{m}{B}]^T \{\overset{m}{\tau}\}\, dV_m \tag{32}$$

where

$$[\overset{m}{k}] \equiv \int_{V_m} [\overset{m}{B}]^T [\overset{m}{A}]\, [\overset{m}{B}]\, dV_m \tag{33}$$

is the element tangent stiffness matrix. Eqs. (15), $(26)^5$, and (32) lead to the following representation of the global stiffness matrix:

$$\left[K\left(t_1\right)\right] = \sum_{m=1}^{M} [\overset{m}{G}]^T \left[\overset{m}{k}\left(t_1\right)\right] \tag{34}$$

The approach used in the finite element solution is to select $[A(t)]$ and $\{\tau(t)\}$ based on the particular ideal model (i.e., constitutive relations) being studied. Then the global stiffness matrix is defined by Eqs. (33) and (34) and the numerical solution proceeds as described previously. Prior to presenting the sample calculations that were performed, the constitutive equation representation for three ideal models is discussed.

Hookian Elastic Model

The "Hookian Elastic" material is represented by the following constitutive equation:

$$T_R^{i\gamma} = F_\alpha^i \left(\frac{K^{\alpha\gamma\beta\delta}}{2} \right) \left(F_\beta^j F_{j\delta} - g_{\beta\delta} \right) \tag{35}$$

where $K^{\alpha\gamma\beta\delta}$ is a constant elastic stiffness tensor and the reference configuration is the natural (i.e., unstressed) configuration.

Eq. (35) is the form appropriate for the present purposes, but it may be transformed easily to the following more recognizable form:

$$\tilde{T}^{\varepsilon\gamma} = K^{\varepsilon\gamma\beta\delta} E_{\beta\delta} \tag{36}$$

In this report the constitutive behavior represented by either Eq. (35), or (36) is what is meant by "Hookian Elastic."

Define $A^{i\gamma}{}_k{}^\varepsilon$ as follows:

$$A^{i\gamma}{}_k{}^\varepsilon \equiv \frac{\partial T_R^{i\gamma}}{\partial F_\varepsilon^k} \tag{37}$$

It follows Eqs. (35), (36), and (37) that

$$A^{i\gamma}{}_k{}^\varepsilon = g_k^i \tilde{T}^{\gamma\varepsilon} + g_{km} F_\alpha^i F_\beta^m K^{\gamma\alpha\varepsilon\beta} \tag{38}$$

$A^{i\gamma}{}_k{}^\varepsilon$ is a tensor representation of $[\overset{m}{A}]$ which is used for the finite element solution procedure for "Hookian Elastic" material. In addition, it follows Eq. (35) that

$$\{\overset{m}{\tau}\} = 0 \tag{39}$$

Isotropic Elastic Model

In this report a specific form of isotropic elastic behavior is selected for this model:

$$T^i_{R\alpha} = \left[K\,(J-1) - \mu\,\frac{I_B}{3J}\right] J\,F^{-1i}_{\alpha} + \mu\,F^i_\alpha \tag{40}$$

where the reference configuration is the natural (unstressed) configuration, K is a scaler bulk modulus, μ is a scaler shear modulus, and

$$J = \text{Det } F$$
$$I_B = \text{tr } F^i_\alpha F^j_\beta g^{\alpha\beta} \tag{41}$$

A clearer representation of the behavior is represented by the Cauchy stress. Eq. (40) is equivalent to the following:

$$T^i_j = \left[K\,(J-1) - \mu\,\frac{I_B}{3J}\right] g^i_j + \frac{\mu}{J}\,B^i_j \tag{42}$$

where

$$B^i_j = F^i_\alpha F^k_\beta g^{\alpha\beta} g_{kj}$$

It follows Eq. (42) that

$$T^k_k = 3K\,(J-1)$$
$$T^i_j - \frac{1}{3}\,T^k_k\,g^i_j = \frac{\mu}{J}\left(B^i_j - \frac{I_B}{3}\,g^i_j\right) \tag{43}$$

It's clear from Eq. (43) that this model represents an isotropic elastic solid and that K and μ are bulk and shear modulii, respectively.

Define $A^{i}{}_{\alpha k}{}^{\varepsilon}$ as follows:

$$A^{i}{}_{\alpha k}{}^{\varepsilon} \equiv \frac{\partial T^{i}_{R\alpha}}{\partial F^{k}_{\varepsilon}} \tag{44}$$

It follows Eqs. (40), (44) that

$$A^{i}{}_{\alpha k}{}^{\varepsilon} = K J \left[(2J - 1) F^{-1}_{k} {}^{\varepsilon} F^{-1}_{\alpha} {}^{i} - (J - 1) F^{-1}_{\alpha k} F^{-1} {}^{\varepsilon i} \right]$$

$$+ \mu \left[g^{i}_{k} g^{\varepsilon}_{\alpha} + \frac{1}{3} \left(I_B F^{-1}_{\alpha k} F^{-1} {}^{\varepsilon i} - 2 F^{\varepsilon}_{k} F^{-1}_{\alpha} {}^{i} \right) \right] \tag{45}$$

$A^{i}{}_{\alpha k}{}^{\varepsilon}$ is a tensor representation of $[\overset{m}{A}]$ which is used for the finite element solution procedure. In addition, it follows Eq. (40) that

$$\{\overset{m}{\tau}\} = 0 \tag{46}$$

Compressible Newtonian Fluid Model

In this report the following constitutive equation represents a compressible Newtonian fluid:

$$T^{i}_{R\alpha} = - \left[\hat{p}(J) J + \frac{2}{3} \mu \dot{J} \right] F^{-1} {}^{i}_{\alpha}$$

$$+ (\mu J) \left(g^{i}_{k} F^{-1} {}^{\beta}_{j} F^{-1} {}^{j}_{\alpha} + F^{-1} {}^{\beta i} F^{-1}_{\alpha k} \right) \dot{F}^{k}_{\beta} \tag{47}$$

where $\hat{p}(J)$ is a scaler valued function and the superposed dot represents the material derivative.

Eq. (47) may be represented in terms of Cauchy's stress tensor using kinematical identities and some algebra:

$$T^{ij} = - \hat{p}(J)\, g^{ij} + \mu \left(L^{ij} + L^{ji} - \frac{2}{3} L^m_m\, g^{ij} \right) \tag{48}$$

where L is the velocity gradient.

Further clarification follows the partitioning of Eq. (48) into the trace of T and the deviator of T:

$$T^m_m = - 3\, \hat{p}(J)$$

$$T^{ij} - \frac{T^m_m}{3} g^{ij} = \mu \left(L^{ij} + L^{ji} - \frac{2}{3} L^m_m\, g^{ij} \right) \tag{49}$$

It follows Eq. (49) that the trace of T is a scaler function of J, the value of $\hat{p}(J)$ is the pressure, there is no bulk viscosity, and shear flow induces shear stress with a constant viscosity μ.

It's convenient to rearrange Eq. (47) for numerical computations. After substituting

$$\dot{J} = J\, \dot{F}^j_\beta\, F^{-1}{}^\beta_j$$

Eq. (47) may be presented as follows:

$$T^i_{R\alpha} = - \hat{p}(J)\, J\, F^{-1}{}^i_\alpha + \mu J \left(g^i_k\, F^{-1}{}^\beta_j F^{-1}{}^j_\alpha + F^{-1}{}^{\beta i}\, F^{-1}_{\alpha k} - \frac{2}{3} F^{-1}{}^\beta_k F^{-1}{}^i_\alpha \right) \dot{F}^k_\beta \tag{50}$$

In the finite element representation it is assumed that the nodal coordinates vary linearly with time during an increment. It follows Eq. (17)[2] that $\dot{F}$ is constant during an increment. Holding $\dot{F}$ fixed in Eq. (50), the time dependence of T_R is seen to be implicit — i.e., depends on $F(t)$ — during an increment. Since $\dot{F}$ is constant during an increment, it may be expressed as follows:

$$F^k_\beta = \frac{\Delta F^k_\beta}{\Delta t} \tag{51}$$

Let $A^i{}_{\alpha k}{}^\beta$ be defined as follows:

$$\begin{aligned} A^i{}_{\alpha k}{}^\beta = &\left[\frac{\partial \hat{p}(J)}{\partial J} J + \hat{p}(J)\right] J F^{-1}_k{}^\beta F^{-1}_\alpha{}^i - \hat{p}(J)\, J\, F^{-1}_{\alpha k} F^{-1}{}^{\beta i} \\ &+ \mu J \left(g^i_k F^{-1}_j{}^\beta F^{-1}_\alpha{}^j + F^{-1}{}^{\beta i} F^{-1}_{\alpha k} - \frac{2}{3} F^{-1}_k{}^\beta F^{-1}_\alpha{}^i \right) \end{aligned} \tag{52}$$

Again $A^i{}_{\alpha k}{}^\beta$ is a tensor representation of $[\overset{m}{A}]$ and it follows Eq. (50) that

$$\{\overset{m}{\tau}\} = 0 \tag{53}$$

2. Sample Problems

Test Case #1

Sample for Hookian Elastic Material

Consider an orthotropic body in plane stress whose elastic modulii are given the following values relative to principal material directions.

$$\begin{aligned} E_{11} &= 10^6 \text{ psi} \quad V_{21} = .1 \quad E_{22} = 10^5 \text{ psi} \\ G_{12} &= .5 \times 10^5 \text{ psi} \quad V_{12} = .01 \end{aligned} \tag{54}$$

In plane stress the stiffness tensor (K) for a Hookian Elastic material may be reduced to two dimensional. The nonzero components of K, which correspond to the values of modulii given by Eq. (54), are

$$K^{1111} = 10^6 \text{ psi} \quad K^{1122} = K^{2211} = 10^4 \text{ psi}$$
$$K^{2222} = 10^5 \text{ psi} \tag{55}$$
$$K^{1212} = K^{1221} = K^{2112} = K^{2121} = .5 \times 10^5 \text{ psi}$$

Now consider the following problem. The body is rectangular with unit width and length three times the width. It is referred to rectangular Cartesian coordinates and is in a natural state at $t = 0$. Loading (traction and boundary motion) is specified as a function of time (i.e., for $t > 0$). At $t = 0$ the body occupies the following space:

$$0 \le X_1 \le 1$$
$$0 \le X_2 \le 3 \tag{56}$$

The problem is specified by the following surface loading:

on $X^1 = 0$ and $X^1 = 1$, surface traction is zero

on $X^2 = 3$, nonzero surface traction is specified:

$$S_R^1(t) = \sin \hat{\theta}(t)\left(1 + 2 \times 10^{-2}t\right)^{1/2}\left(10^3 - 1\right)t$$
$$S_R^2(t) = \cos \hat{\theta}(t)\left(1 + 2 \times 10^{-2}t\right)^{1/2}\left(10^3 - 1\right)t$$

on $X^2 = 0$, motion is specified: (57)

$$x^1(t) = \cos \hat{\theta}(t)\left(1 - 2 \times 10^{-4}t\right)^{1/2} X^1$$
$$x^2(t) = - \sin \hat{\theta}(t)\left(1 - 2 \times 10^{-4}t\right) X^1$$

Figure 1 illustrates the surface loadings.

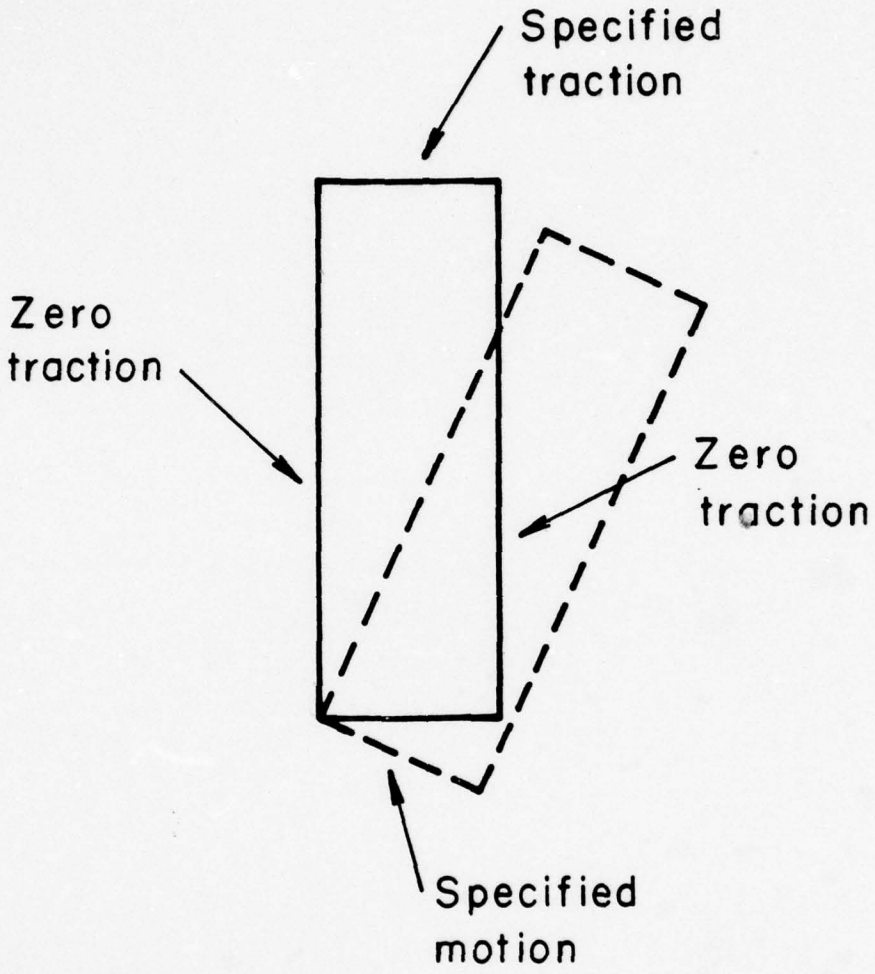

Figure 1. Surface loadings for Test Case #1.

The following motion is an exact solution to the stated problem.

$$
\begin{aligned}
x^1(t) &= \cos\hat{\theta}(t)\left(1 - 2\cdot 10^{-4}t\right)^{1/2} X^1 \\
&\quad + \sin\hat{\theta}(t)\left(1 + 2\cdot 10^{-4}t\right)^{1/2} X^2 \\
x^2(t) &= -\sin\hat{\theta}(t)\left(1 - 2\cdot 10^{-4}t\right)^{1/2} X^1 \\
&\quad + \cos\hat{\theta}(t)\left(1 + 2\cdot 10^{-4}t\right)^{1/2} X^2
\end{aligned}
\tag{58}
$$

The deformation gradient and stress are easily computed from the motion given by Eq. (58) and the stiffness tensor.

The problem represented by Eq. (57) was solved numerically using the finite element technique described earlier. It was run for a duration of 1 sec. Several variations were run, each with a constant rate of rotation — i.e., represented by $\hat{\theta}(t)$. The rates of rotation studied ranged from zero to 90°/sec. Also of interest is the tradeoff between time step (i.e., increment size) and the number of iterations required for convergence. The convergence criterion used is that the iterative change in each nodal coordinate be less than .1% of the maximum coordinate change during the time step. Figure 2 presents the finite element model used in the study, and Table 1 summarizes the convergence study.

The accuracy obtained is excellent. A comparison of the numerical results and analytic solution for $\dot{\theta} = 30°/\text{sec}$ is presented by Figure 3.

Test Case #2

Generalized Shear

Green and Atkins[5] present an analytic solution for "Generalized Shear" of an isotropic incompressible elastic material, defined by the following constitutive equation:

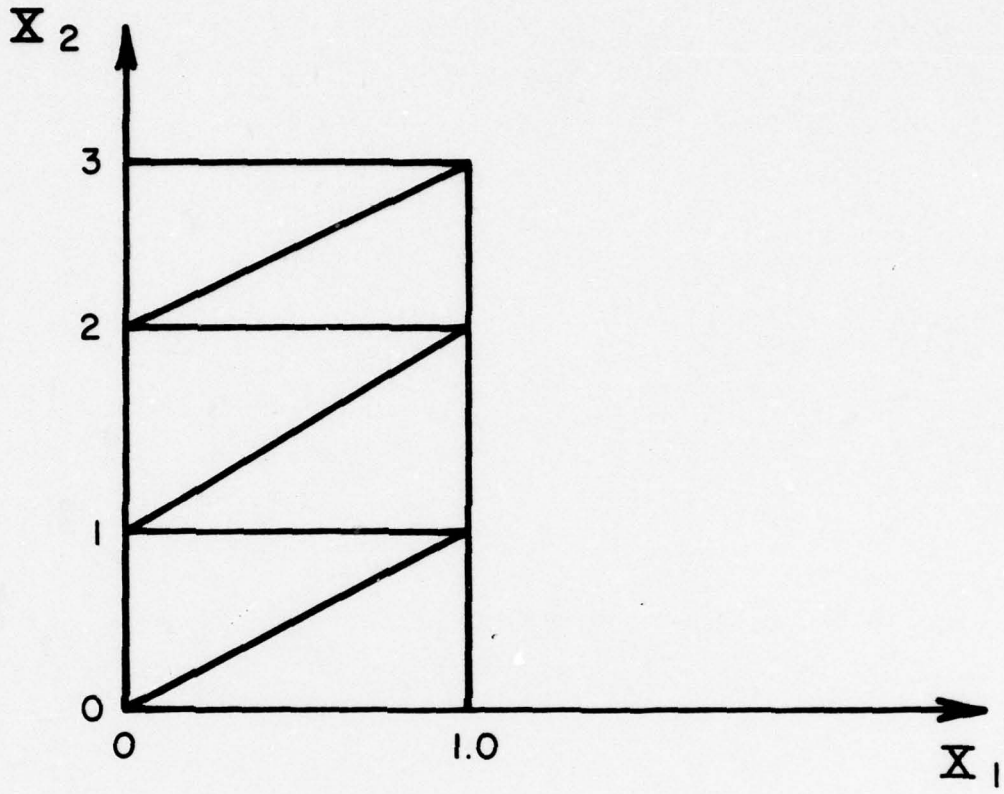

8 Nodes
6 Elements
16 Degrees of Freedom

Figure 2. Test Case #1 - finite element model.

TABLE 1

TEST CASE #1

NUMERICAL SOLUTION TABLE OF CONVERGENCE

ROTATION RATE (DEG/SEC)	TIME STEP (SEC)	NUMBER OF ITERATIONS
0	.05	3
15		5
30		8
45		14
60		28
90		> 75
30	.05	8
	.10	30
	.15	> 75
	1	∞

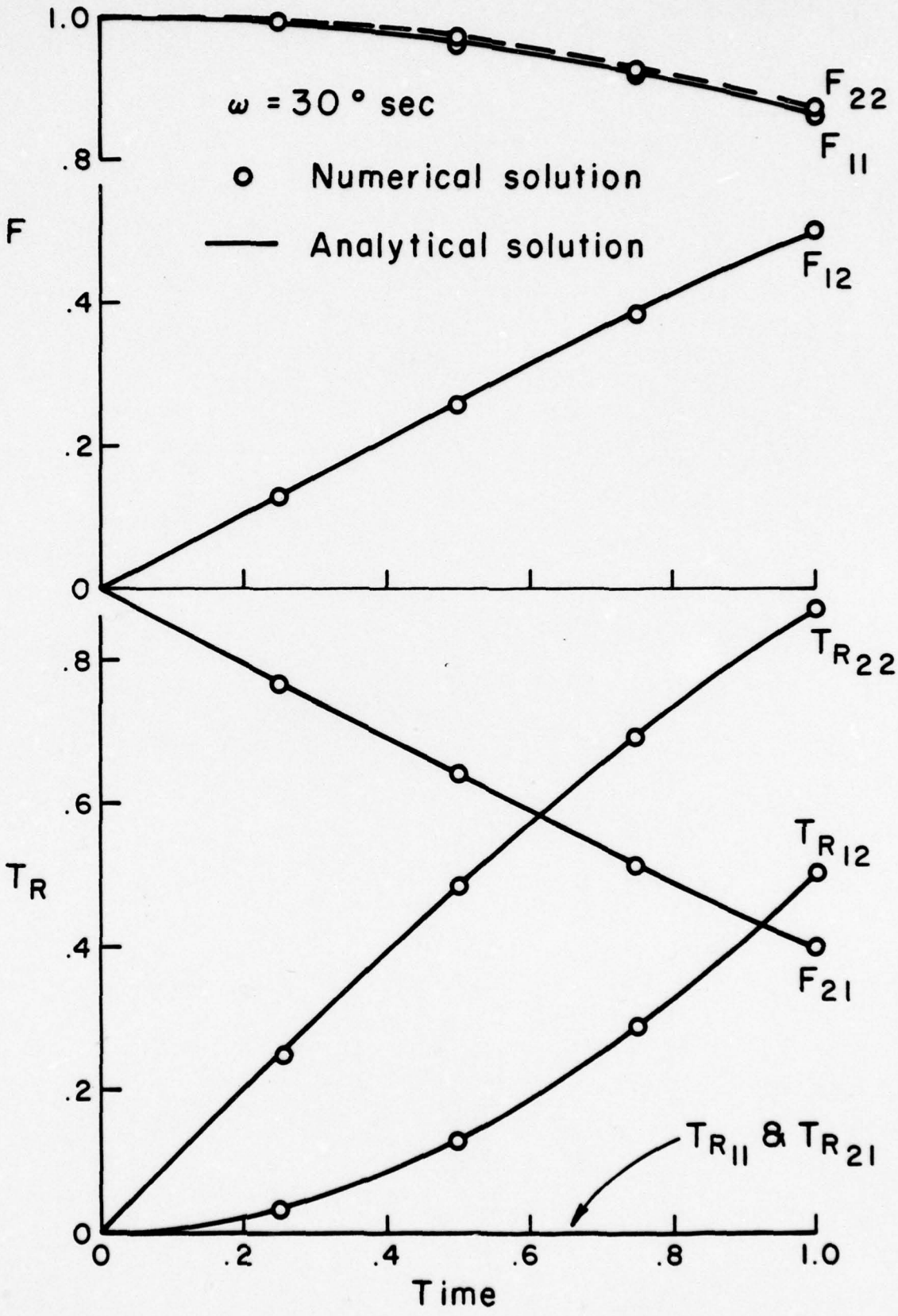

Figure 3. Test Case #1 - numerical solution.

$$T_R^{i\alpha} = - p F^{-1}{}^{\alpha i} + \mu F^{i\alpha} \tag{59}$$

where the deformation is restricted so that Det F = 1 , and p is a scaler which is independent of straining. Now consider a rectangular two-dimensional body subject to plane deformation. At t = 0 the body is in a natural state and occupies the following space:

$$\begin{aligned} 0 \le X^1 \le .25\,L \\ 0 \le X^2 \le L \end{aligned} \tag{60}$$

On the four boundaries the following loading is specified as a function of dimensionless time:

on $X^2 = 0$ the boundary is fixed

on $X^2 = L$

$$S_R^1(t) = \mu \frac{t}{2}$$

$$S_R^2(t) = - \mu \left[\left(\frac{X_1}{L} \right) \frac{t}{2} + \frac{1}{8} t^2 \right]$$

on $X^1 = 0$ (61)

$$S_R^1(t) = \frac{\mu}{8} \left(\frac{X^2}{L} \right)^2 t^2$$

$$S_R^2(t) = - \mu \left[1 + \frac{1}{8} \left(\frac{X^2}{L} \right)^2 t^2 \right] \frac{1}{2} \left(\frac{X^2}{L} \right) t$$

on $X^1 = .25\,L$

$$S_R^1(t) = - \frac{\mu}{8} \left[t + \left(\frac{X^2}{L} \right)^2 t^2 \right]$$

$$S_R^2(t) = \frac{\mu}{2} \left(\frac{X^2}{L} \right) t \left[1 + \frac{t}{8} \left(1 + \left(\frac{X^2}{L} \right)^2 t \right) \right]$$

Figure 4 illustrates the surface loadings.

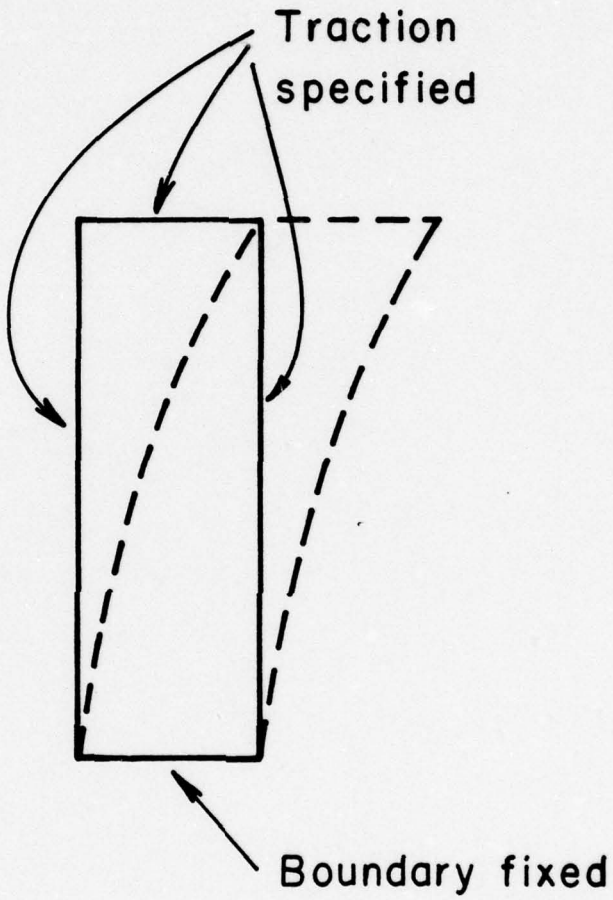

Figure 4. Test Case # 2 - surface loadings.

An analytic solution to the problem given by Eq. (61) is given by the following:

$$\frac{x^1(t)}{L} = \left(\frac{X^1}{L}\right) + \frac{1}{4}\left(\frac{X^2}{L}\right)^2 t$$

$$\frac{x^2(t)}{L} = \frac{X^2}{L} \tag{62}$$

$$\frac{x^3(t)}{L} = \frac{X^3}{L}$$

$$\frac{T_R^{11}(t)}{\mu} = -\left[\frac{1}{2}\left(\frac{X^1}{L}\right) t + \frac{1}{8}\left(\frac{X^2}{L}\right)^2 t^2\right]$$

$$T_R^{22}(t) = T_R^{33}(t) = T_R^{11}(t) \tag{63}$$

$$\frac{T_R^{12}(t)}{\mu} = \frac{1}{2}\left(\frac{X^2}{L}\right) t$$

$$\frac{T_R^{21}(t)}{\mu} = \left[1 + \frac{1}{2}\left(\frac{X^1}{L}\right) t + \frac{1}{8}\left(\frac{X^2}{L}\right)^2 t^2\right]\left(\frac{X^2}{L}\right)\frac{t}{2}$$

The problem represented by Eq. (61) was solved numerically using the finite element solution technique described earlier. The constitutive equation presented by Eq. (59) is an approximate representation of rubbery materials and is restricted to isochoric deformations. For the numerical study the constitutive equation presented by Eq. (40) was used. In rubbery material the ratio of bulk modulus to shear modulus is of the order of 10^4, therefore in the numerical study

$$\frac{K}{\mu} = 10^4 \tag{64}$$

The finite element model used for this study is presented by Figure 5. The problem was run for a duration of $t = 1$. The tradeoff between time step size and the number of iterations required for convergence is summarized by Table 2. A 1% convergence tolerance means the solution for any time step was iterated until the change in each nodal coordinate from an iteration was less than 1% of the maximum value of any nodal displacement during that time step. The numerical results compared excellently with the analytic solution. For example, the comparison of three parameters is given by Figure 6. ϕ is the angle illustrated by the sketch on the figure, Q is the x^1 coordinate of the top corner node, and T_R^{12} is computed at the centroid of the upper most right element on Figure 5.

Test Case #3

Pure Shearing Flow of a Compressible Newtonian Fluid

Consider the plane flow represented by

$$\begin{aligned} v^1 &= - a x^1 \\ v^2 &= + a x^2 \qquad \text{for} \quad t \geq 0 \\ v^3 &= 0 \end{aligned} \tag{65}$$

where a is constant and v is the particle velocity.

Such a flow is possible in a Newtonian fluid and the corresponding stresses are computed using Eq. (48):

$$\begin{aligned} T^{11} &= - \hat{p}(J) - 2\mu a \\ T^{22} &= - \hat{p}(J) + 2\mu a \\ T^{33} &= - \hat{p}(J) \\ T^{12} &= T^{23} = T^{31} = 0 \end{aligned} \tag{66}$$

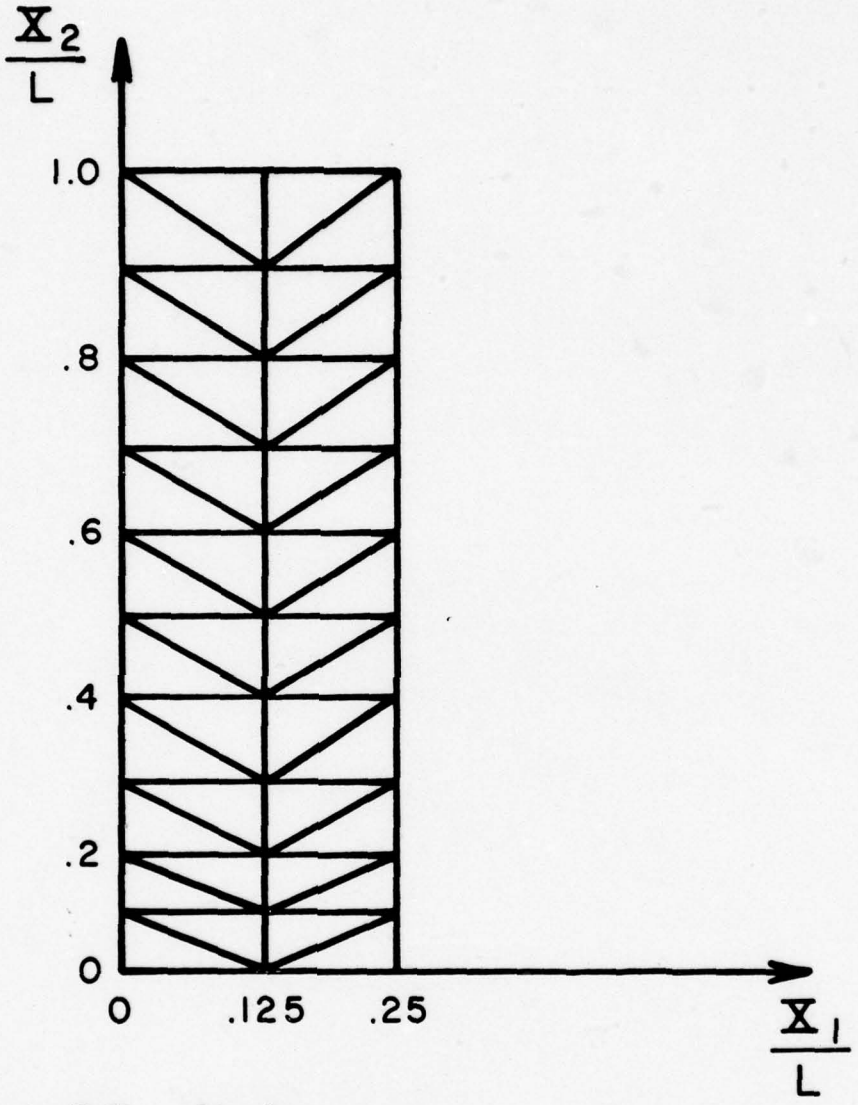

Figure 5. Test Case #2 - finite element model.

TABLE 2

TEST CASE #2

NUMERICAL SOLUTION TABLE OF CONVERGENCE

TIME STEP	CONVERGENCE TOLERANCE	NUMBER OF STEPS	AVG ITERATIONS PER STEP
.001	1%	1000	3
.01	↓	100	5
.02	↓	50	7
.025	↓	40	8
.04	↓	-	> 50
.05	↓	-	> 50
1.0	↓	-	BLOWS UP

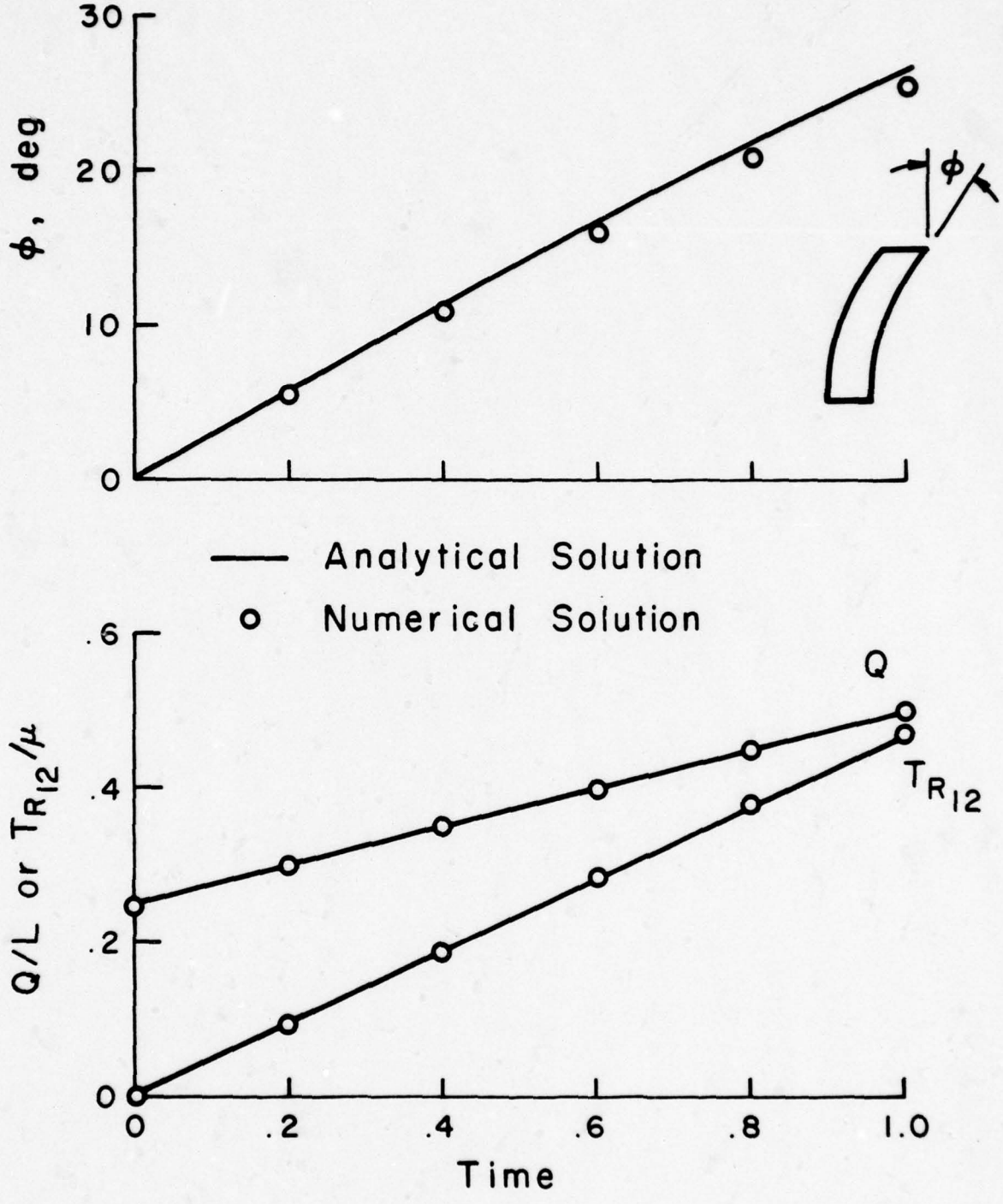

Figure 6. Test Case #2 - numerical solution.

Now consider a rectangular body subject to plane deformation. Let the body occupy the following space at $t = 0$:

$$0 \le X^1 \le 1.5$$
$$0 \le X^2 \le 2 \tag{67}$$

with the initial velocity field given by

$$v^1 = - a X^1$$
$$v^2 = a X^2 \qquad \text{at} \quad t = 0 \tag{68}$$

Furthermore subject the boundaries of the body to the following mixed specification for $t > 0$.

$$\text{on} \quad X^1 = 0 \quad v^1 = 0 \quad S^2_R = 0$$
$$\text{on} \quad X^1 = 1.5 \quad v^1(t) = - 1.5\, a e^{-at}$$
$$S^2_R = 0$$
$$\text{on} \quad X^2 = 0 \quad v^2 = 0 \quad S^1_R = 0 \tag{69}$$
$$\text{on} \quad X^2 = 2 \quad v^2(t) = 2 a e^{at}$$
$$S^1_R = 0$$

Figure 7 illustrates the surface motion specified.

It can be shown that the problem stated by Eqs. (67), (68), (69) has a solution given by Eq. (65) with stresses given by Eq. (66). It also follows that the motion of the body depends only on the motion specified at the boundaries and is independent of the viscosity μ . In terms of material coordinates the motion is given by the following:

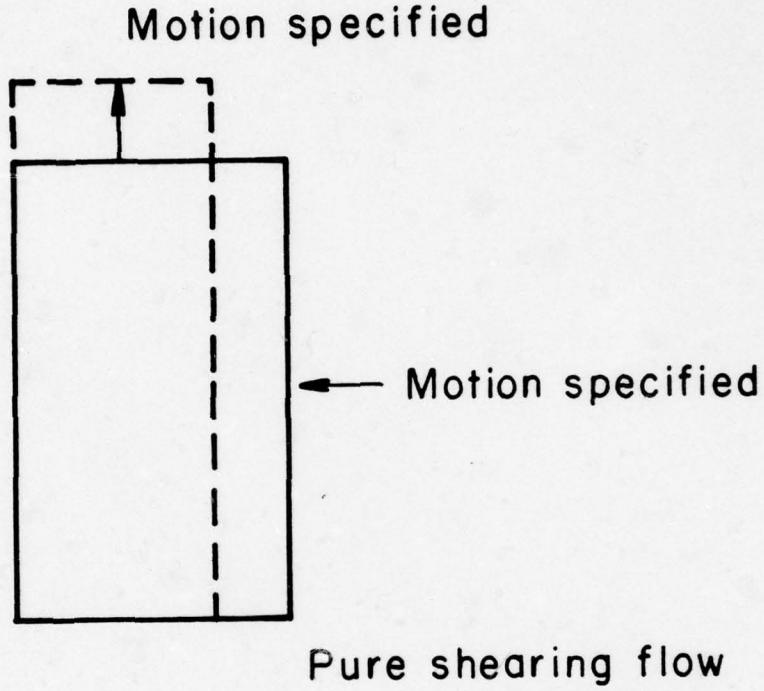

Figure 7. Test Case #3 - surface motion.

$$x^1 = X^1 e^{-at}$$
$$x^2 = X^2 e^{at} \qquad (70)$$

It follows Eq. (70) that the deformation gradient is given by the following:

$$F^{11} = e^{-at}$$
$$F^{22} = e^{at} \qquad \text{for} \quad t \geq 0 \qquad (71)$$
$$F^{12} = F^{21} = 0$$

The problem defined by Eqs. (67), (68), (69) was solved numerically using the finite element technique described earlier. It was run for a duration of 1.2 sec with $a = .5/\text{sec}$. The finite element model used is presented by Figure 8. The numerical results compared excellently with the analytic solution. To illustrate, the comparison is given for some of the parameters by Figure 9. The values of F^{11} , F^{22} are taken from one of the elements, and Q_{11} , Q_{12} are the current coordinates of one of the interior nodes.

Test Case # 4

Growth of an Elliptic Cavity

In 1962, Berg[6] presented the results of an interesting study: "The Motion of Cracks in Plane Viscous Deformation." This paper is the basis for the choice of this sample problem. The problem is especially suited for the present study because it involves following a deforming free-surface in a fluid body.

The problem is illustrated by Figure 10. An infinite sheet of material is subject to pure shear stress at infinity. At $t = 0$ there exists an elliptically shaped cavity. The material

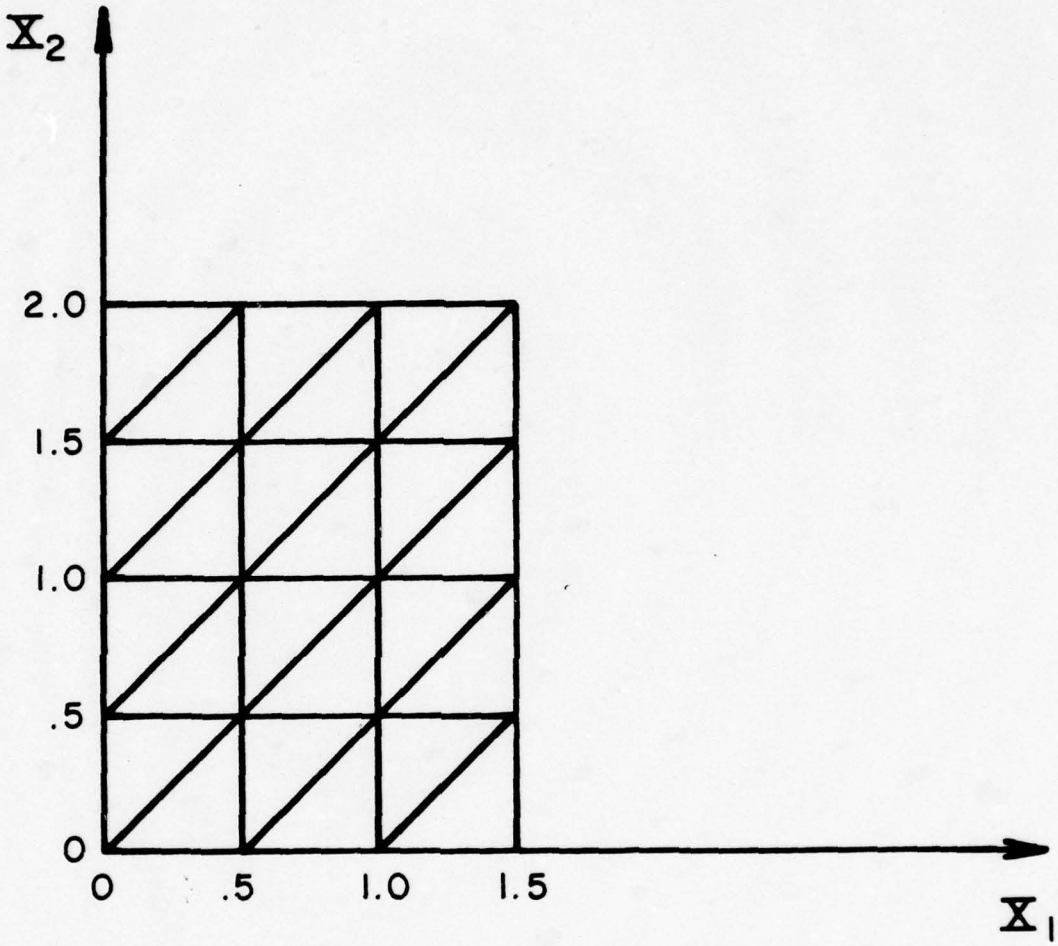

20 Nodes
24 Elements
40 Degrees of Freedom

Figure 8. Test Case #3 - finite element model.

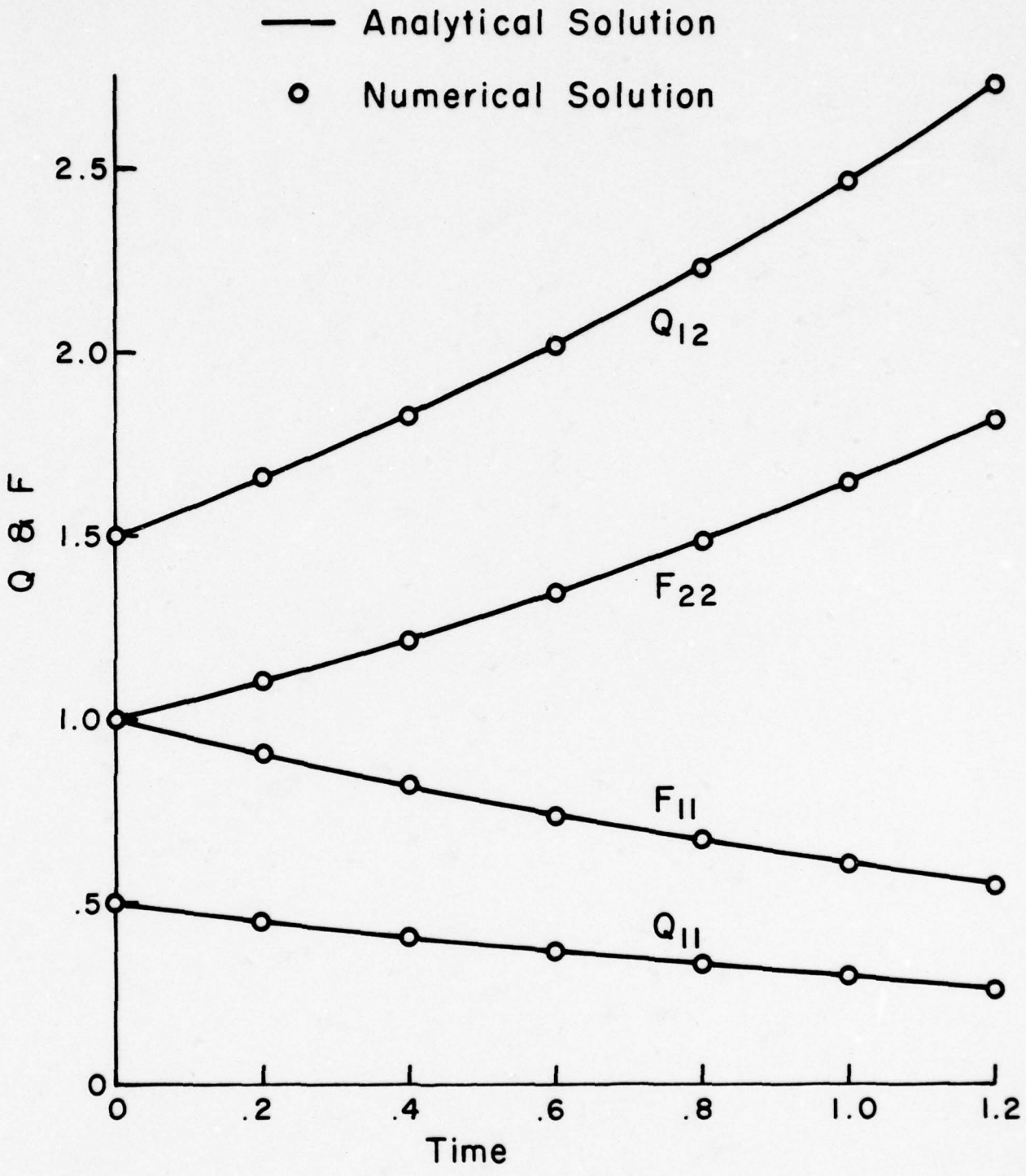

Figure 9. Test Case #3 - numerical solution.

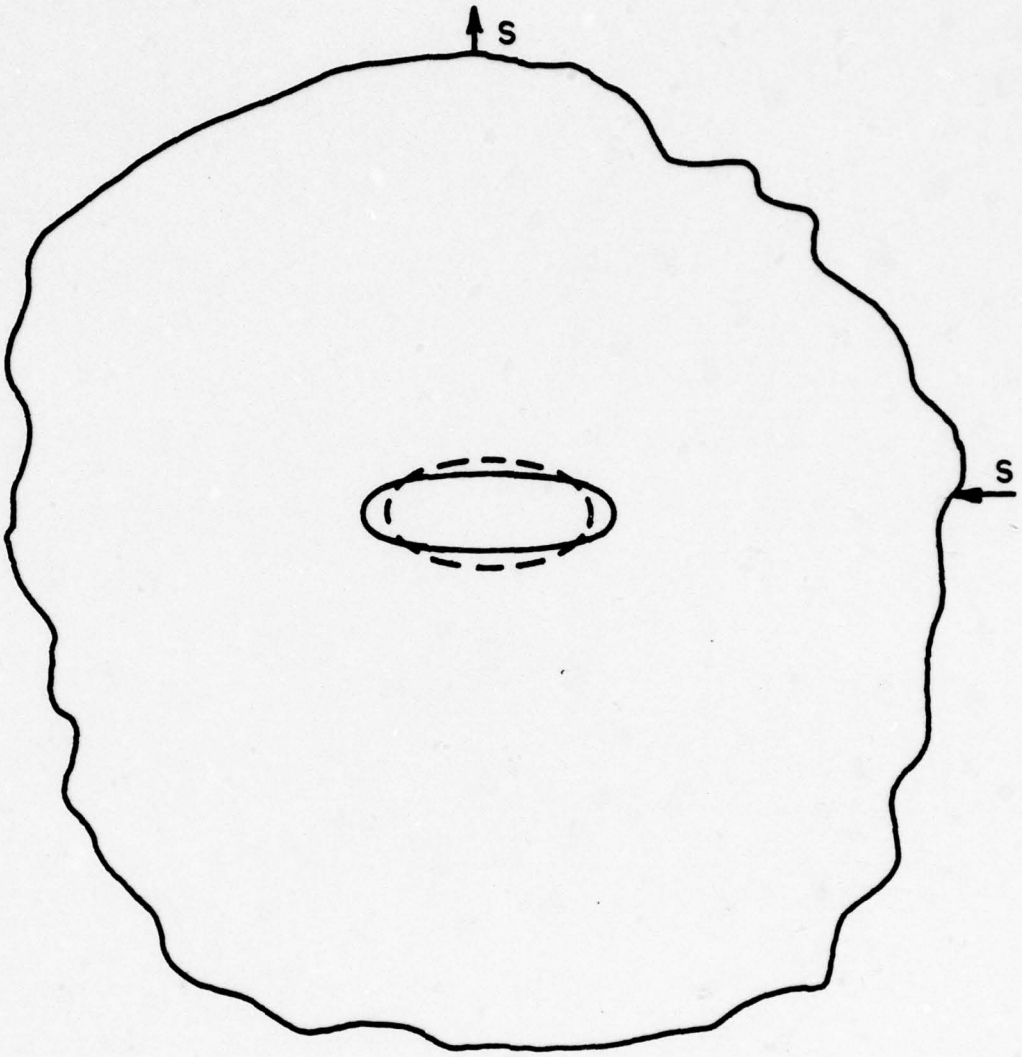

Figure 10. Test Case #4 - growth of elliptic cavity subject to plane creeping flow.

is characterized as an incompressible Newtonian fluid. The stress at infinity is held constant and the motion of the cavity is studied. Berg shows that an elliptical cavity remains elliptical always. Also, it follows Berg's analysis that the flow at infinity (for pure shear stress) preserves the area of the infinite sheet. Since the constitutive behavior is incompressible, is is concluded (here) that the area of the cavity must be preserved. If we let $a(t)$, $b(t)$ represent the semi-axes of the ellipse it follows that the solution must satisfy

$$a(t)\, b(t) = \text{constant} \tag{72}$$

A form convenient for checking numerical results is obtained by differentiating Eq. (72):

$$-\frac{\dot{a}(t)}{\dot{b}(t)} = \frac{a(t)}{b(t)} \tag{73}$$

It's difficult to gleam more quantitative data from the analytical solution.

The problem was studied numerically using the compressible Newtonian fluid model. The bulk becavior was assumed given by the the following:

$$\hat{p}(J) = 10^5 \text{ psi } (1 - J) \tag{74}$$

Obviously an infinite body cannot be modeled. The finite element model used is shown by Figure 11. Note the break in the coordinates and that the advantages of symmetry are utilized. To simulate the motion at infinity the following motion was specified for each node located on the outer ring of the model:

$$\begin{aligned} v^1(t) &= -\frac{1}{2} X^1 e^{-t/2} \\ v^2(t) &= +\frac{1}{2} X^2 e^{+t/2} \end{aligned} \tag{75}$$

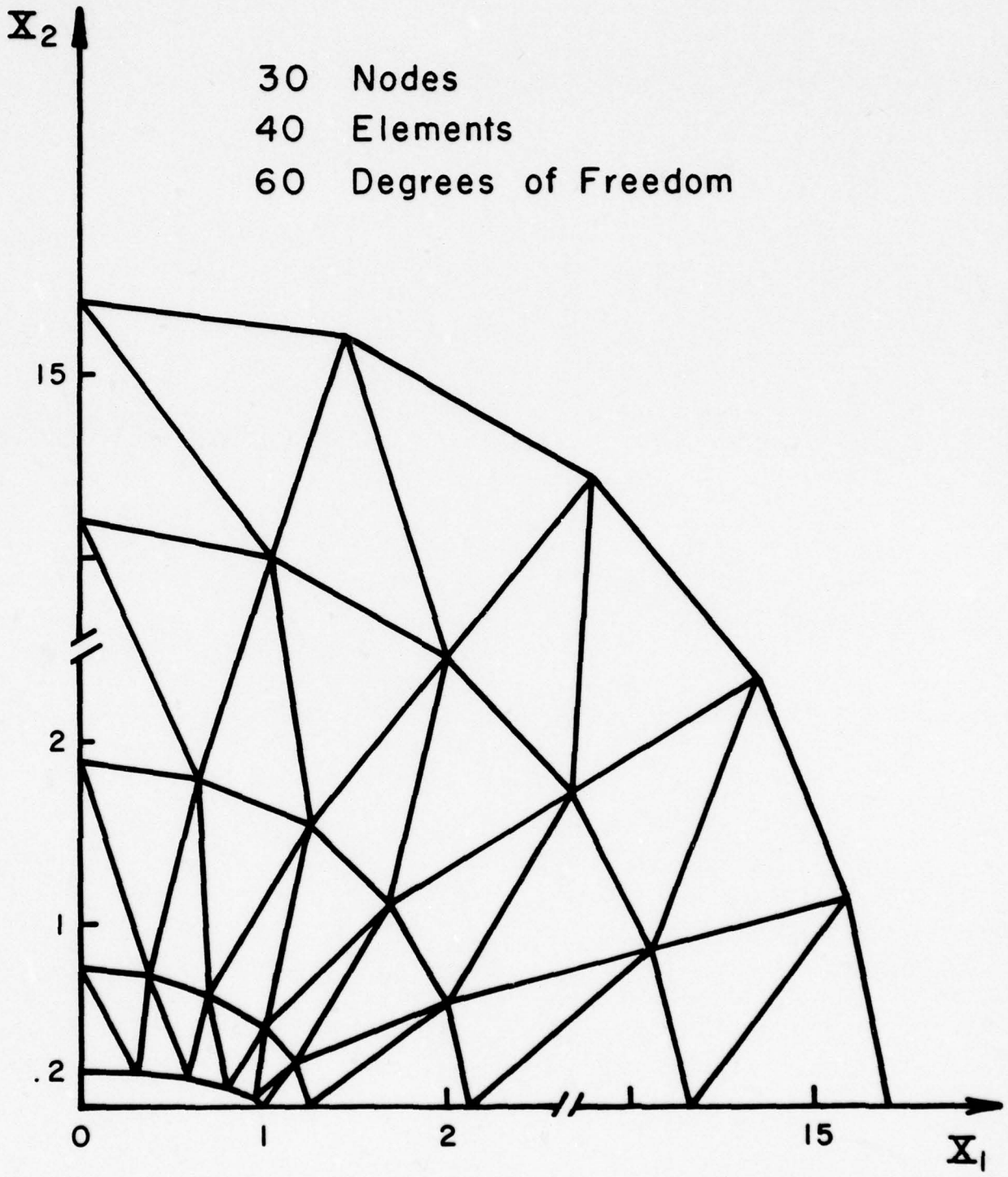

Figure 11. Test Case #4 - finite element model.

The initial nodal velocities were assumed zero; this is obviously not the correct initial conditions for the problem but the correct conditions were not available. Some of the results are summarized by Figure 12. The lower figure illustrates the cavity shape for three values of time. The upper figure illustrates how well Eq. (73) is satisfied by the numerical results; Q_{10} and Q_1 are the nodal coordinates whose values correspond to the semi-axes of the elliptical cavity. Note the inaccuracy at very early time due to the inaccurate initial values. The correlation appears good for later times.

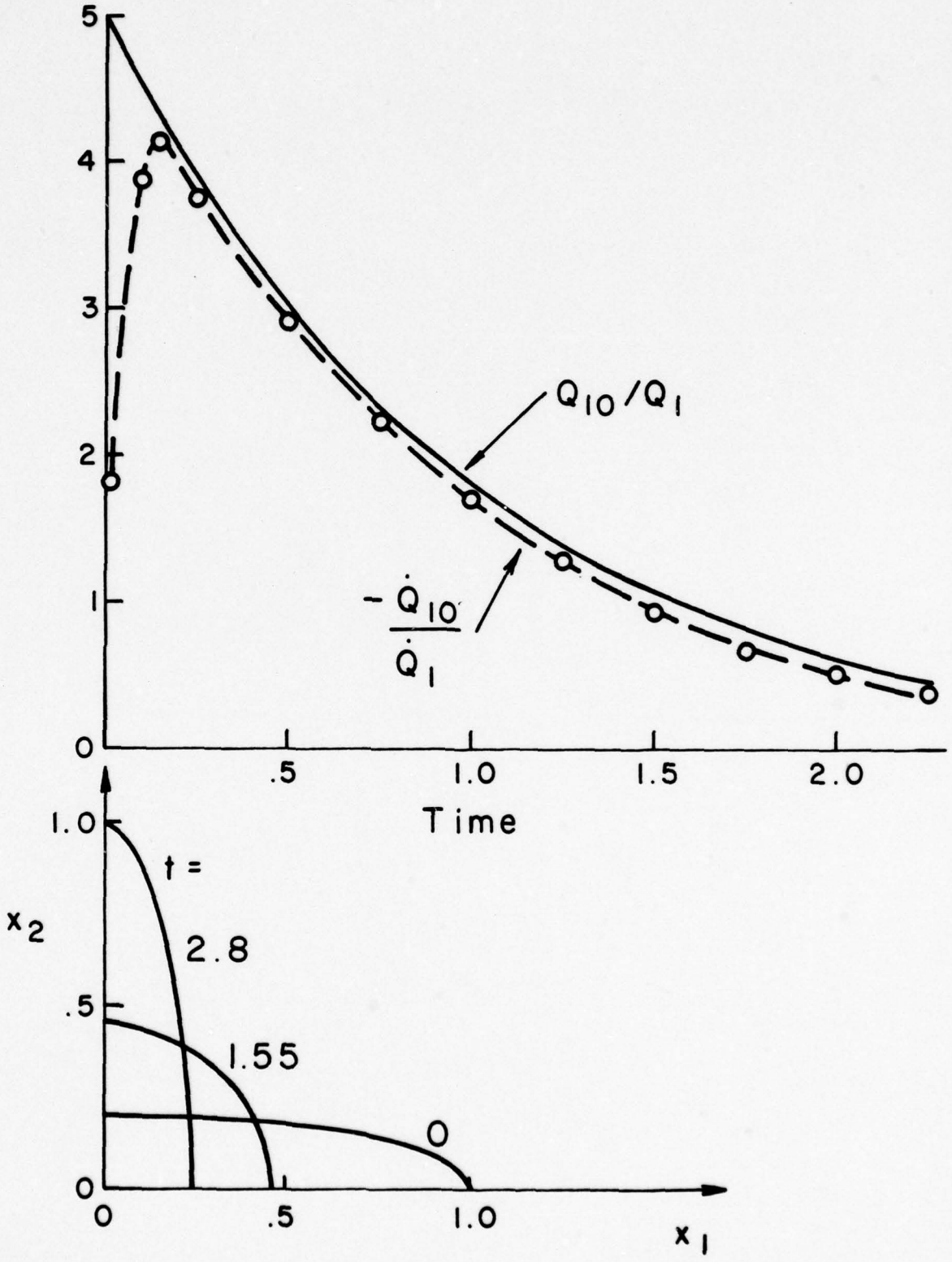

Figure 12. Test Case #4 - numerical solution.

III. RESIDUAL STRESS ANALYSIS

1. Technical Overview

A principal reason which motivates the study of residual stress is to improve the quality of modern composite materials and their application to component design. The mechanical characteristics (strength, stiffness, toughness, etc.) are measurable properties which are very sensitive to "quality"; therefore they are frequently used as indicators, besides they are of-themselves of primary importance to component design for many applications. Hopefully, further study of the development of residual stress during processing will lead to increased understanding. This knowledge can be applied to the design of processes which yield better quality material.

The magnitude of residual stress that exists in a component which is made up of composite material depends on physical changes that occur in the constituents during processing and the geometric arrangement of the constituents (i.e., laminate layup, three-dimensional weave, etc.). These two contributors represent quite different phenomena and may be understood best when discussed individually.

The physical changes that occur in the constituents may be quite different when comparing different composite systems, but each can be reduced to a single common parameter which is essential to residual stress development. The essential parameter is the dimensional change experienced by the constituents. Examples are the shrinkage of a resin as a result of polymerization, the shrinkage of liquid metal on solidification, growth of graphite fibers (due to annealing) during graphiterization cycles, differential thermal expansion on cooling to room temperature, etc.

The other contributor is due to the geometry of the constituents' arrangement and their different mechanical properties. As

far as predicting stresses is concerned, it is both convenient (from a computational viewpoint) and enlightening (from an understanding viewpoint) to perform different levels of analysis: micromechanics and macromechanics. In micromechanics, the heterogeneous nature of a material is recognized, and stresses in individual constituents may be identified. On the other hand, macromechanics describes a material as homogeneous and uses effective properties to represent its elastic behavior. In this approach, the stress is interpreted as average (on an area larger than microdimensions), and no information about constituent stresses is obtained.

It's useful to partition the analyses of residual stress into two types, which are called here Predictive and Descriptive. By "Predictive Analysis" is meant a theoretical/numerical prediction of residual stresses which does not utilize residual strain measurements in the component under study. There are many published experimental studies of residual stress; these are called here Descriptive. Descriptive analyses always involve an experiment performed on a particular component. Generally only strains can be measured and theoretical/numerical predictions are required to interpret the data in terms of stress. Clearly, both types of analyses have shortcomings, but both contribute toward improved understanding. The publications of Shaffer and Levitsky[7,8] represent an ambitious approach toward a predictive analysis. Examples of predictive analysis in use for modern composite materials are published by Chamis[9]. Descriptive analyses of interest are found in the publications of Marloff and Daniel[10], Koufopoulos[11] Daniel and Liber[12], and Lee, Sacher, and Lewis[13].

It's impossible to perform a predictive analysis with assuming a model to represent the physical-chemical processes at work during the fabrication of a component — even if the assumption is only implied by the retention and neglect of various phenomenon. In order to be definitive the following describes a model assumed here for resin reinforced composite materials:

1) The resin is in a green stage when a component is laid up, and prior to curing the component is stress-free.

2) Curing is performed under controlled pressure at elevated temperatures (frequently in the range of 300 to 400 °F).

3) During the cure time the resin polymerizes. When the component is first heated to the cure temperature the degree-of-polymerization (D-O-P) is low and the resin flows easily. With time the D-O-P advances and the resin viscosity increases, making it gradually more difficult for the resin to flow. Simultaneously the stress-free volume of the resin decreases (or increases) as the D-O-P advances, and it is assumed the dimensions of the reinforcement are stable.at the cure temperature. Consequently, the resin shrinkage induces stresses in the component. Finally, with sufficient time, the polynerization is complete and the final stress distribution in the component depends on the history of shrinkage and viscosity in addition to the geometry and modulii of the reinforcement.

4) After the completion of polymerization the component is cooled to room temperature and the pressure applied to the component is relieved. During the cool-down the two constituents undergo unequal thermal contraction. The resulting incompatible dimensional changes during the cool-down induce further stress

5) The residual stress is the stress remaining in the component at room temperature. It is a result of incompatible dimensional changes which are a consequence of both "polymerization changes" and "cool-down."

No one doubts the importance of cool-down for the consideration of residual stresses. It is the only phenomenon considered

in predictive analyses of modern composite materials. On the contrary the effects of polymerization are ignored generally — not through ignorance necessarily. Many of the researchers believe that creep or relaxation of the resin at cure temperature is sufficient so that the stresses developed during polymerization are negligible; at least this appears to be a common opinion for epoxy resin. Yet there appears to be little evidence in the available descriptive analyses to support such an assumption.

The conclusion (made here) that the effects of the polymerization change have not been identified in descriptive analyses is not immediately obvious upon reviewing the available documentation. On first reflection one easily may think that the results of Daniel and Liber[12] measure directly the effects of the polymerization change. They implanted strain gages between the lamina of a laminate in the green stage and monitored strain output during the polymerization of the resin. The following idealized description of the phenomena sheds doubt on the usefulness of the imbedded strain gage as a measure of polymerization changes.

The idealized model is illustrated schematically by Figure 13. The sketch on the upper right illustrates that the viscosity of the resin increases with time during curing (i.e., implicitly through D-O-P) and the stress-free volume decreases with time. The sketch on the upper left suggests that for a period (say $t < t_1$) the resin flows readily; therefore, stresses due to the incompatibility are relaxed quickly. Suppose at time $t = t_1$ the viscosity has grown sufficiently so that further development of stress is retained, i.e., further straining of the resin is constrained by the fibers. Suppose the stress-free volume is V_1 at $t = t_1$ and V_F is the value for fully cured resin. It follows that the final residual stress will be proportional to $V_F - V_1$. The uniaxial strain corresponding to $V_F - V_1$ is not observable to the imbedded strain gage; $V_F - V_1$ is a mechanical

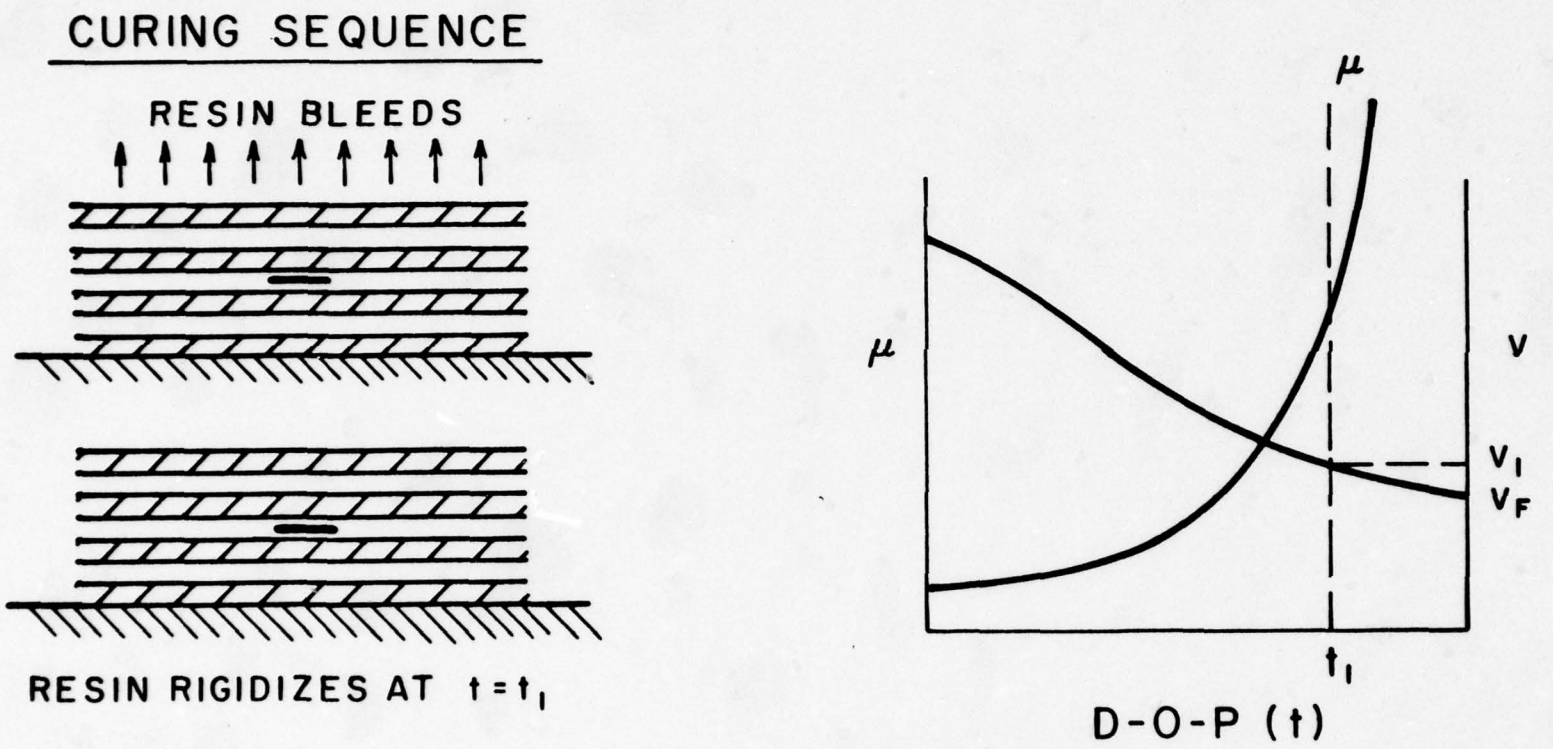

Figure 13. Embedded strain gage assessment.

strain of the resin which is prevented from occurring by the much stiffer fibers. Hence, the residual stress developed during polymerization is due to a lack of (potential) straining which would occur were it not for the constraint of the stiffer fibers. Imbedded strain gages sense only the (total) strain that does occur; therefore, such strain data is insensitive to the residual stress that develops during polymerization

In the absence of direct descriptive analyses, other indicators of the importance, or unimportance, of polymerization changes may be sought. For example, the total incompatibility may be assessed in the absence of relaxation. If the total incompatibility is unimportant for a particular resin, it appears safe to ignore it. Such an assessment is summarized by Table 3.

Three resins were selected. Epoxy and phenolic are two resins for which there is considerable processing experience and interest. Polyimide is selected because presently there is considerable interest in its application. ε^T is the uniaxial thermal expansion of the resin due to cooling from the deposition temperature to room temperature, ε^P is the uniaxial dimensional change due to polymerization, and ε_F^T is the uniaxial thermal expansion of the reinforcement due to cooling from the curing temperature to room temperature. Of the properties used in Table 3, ε^P is the least available. The value used for epoxy is obtained from Emerson & Cuming Inc. (Catalog) for Stycast 1269A. The value used for phenolic is an estimate based on private communication with Dr. Paul Juneau (General Electric Company, Switchgear Equipment Business Division). No estimate was obtained for polyimide even though several researchers were contacted (e.g., Mr. Benson Dexter, NASA-LRC; Dr. Terry Saint Clare, NASA-LRC; Dr. Tito Serafini, NASA-Lewis; and Dr. Joe Augl, NSWC-WOL).

The incompatibility due to cool-down is proportional to the differential thermal expansion $\Delta\varepsilon^T = \varepsilon^T - \varepsilon_F^T$ and that due to

TABLE 3. ASSESSMENT OF POLYMERIZATION DIMENSIONAL CHANGE

MATRIX	PROCESS TEMPERATURE (°F)	UNIAXIAL THERMAL EXPANSION ε^T (IN/IN)	POLYMERIZATION DIMENSIONAL CHANGE ε^P (IN/IN)	$\varepsilon^P/\varepsilon^T$	FIBER	ε_F^T (IN/IN)	$\Delta\varepsilon^T$ (IN/IN)	$\varepsilon^P/\Delta\varepsilon^T$
EPOXY (UNFILLED)	350	-.01	-.006	.6	BORON	-.00060	-.00940	.64
					CARBON	-.00275	-.00725	.83
					GRAPHITE	-.00220	-.00780	.77
					QUARTZ	-.000825	-.00918	.65
PHENOLIC	350	-.0165	-.064	3.88	BORON	-.00060	-.0159	4.03
					CARBON	-.00275	-.0137	4.67
					GRAPHITE	-.00220	-.0143	4.48
					QUARTZ	-.000825	-.0157	4.08
POLYIMIDE		-	UNKNOWN					

polymerization is represented by ε^P . The ratio of ε^P to $\Delta\varepsilon^T$ (shown in the last column) is a measure of the importance of polymerization relative to the cool-down. For the reinforcements considered the polymerization changes for epoxy resin are in excess of 60% of that due to cool-down and for phenolic resin are in excess of 400% of that due to cool-down. It follows that the contribution of polymerization changes to the residual stress cannot be shown negligible on the basis of a conservative estimate such as summarized by Table 3.

2. Predictive Analysis

This section summarizes an initial step toward the development of a predictive analysis for resin reinforced composite materials. The approach taken is to develop a micromechanical analysis (i.e., the resin and reinforcement are distinguished in the analysis). It's assumed that the phenomena which occur during polymerization are "slow"," so that the approximations of creeping flow are appropriate; in this case the equations-of-motion reduce to equilibrium equations. The physical-chemical processes that occur during the curing of the resin — and are responsible for the development of stress during that time — are reflected by the constitutive equations which are selected to represent the resin behavior. The finite element technique, which is described in the first section of this report, is used to perform numerical studies. The other field equations, besides the constitutive equation, are contained inherently in the finite element technique and need no special attention here.

The following list is a goal for the phenomena to be represented by the constitutive equations:

1) The reinforcement is dimensionally stable at the cure temperature and behaves elastically.

2) The resin starts liquid-like with low viscosity; the viscosity increases with advance of D-O-P until at the end of cure the resin behaves solid-like.

3) The stress-free volume of the resin varies continuously with the D-O-P.

It is useful to represent time-dependent models of mechanical behavior by springs and dash-pots. The following sketch illustrates pictorially a representation of the phenomenon described above:

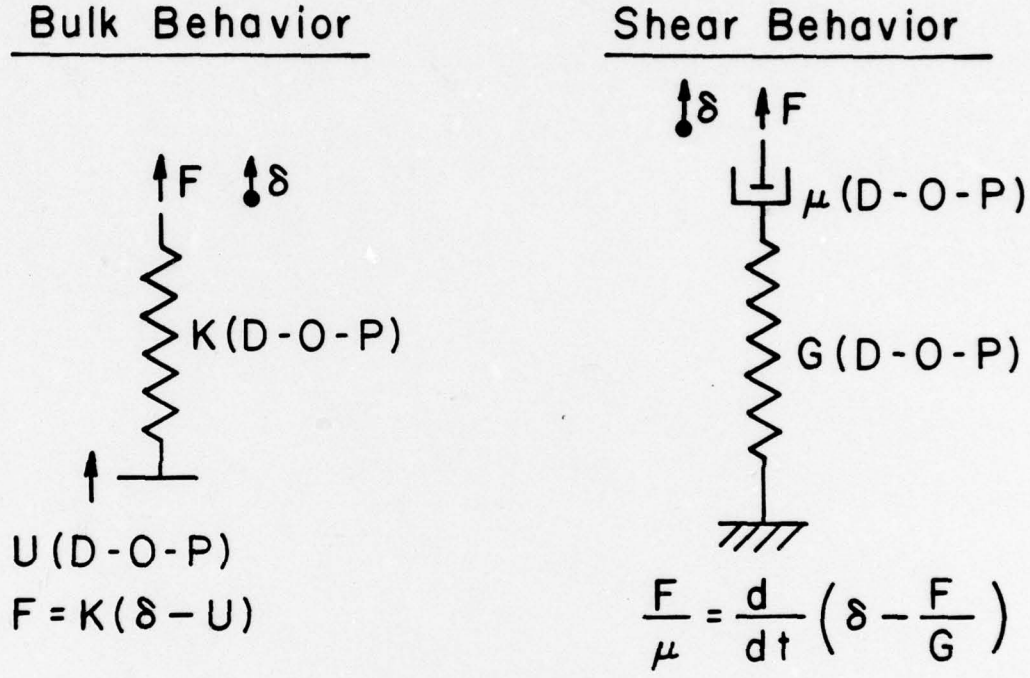

In the representation of bulk behavior the bulk modules (K) may depend on the D-O-P, and the base movement (-U) represents the change of stress-free volume with D-O-P. In shear the transition from fluid-like to solid-like behavior is controlled primarily by the viscosity μ. For small μ the model will creep readily under applied stress, and the elastic recovery will be very small. For very large μ an increment of strain is accommodated by stretch of the spring, which can be recovered elastically. Actually, the magnitude of μ, small or large, must be measured relative to the magnitude of G and a measure of time.

The choice of a multiaxial invariant constitutive equation, for which the spring and dash-pot model above is an analogue, is not unique. Following Eq. (43), B is selected as the measure of strain and the corotational derivative is selected for the time flux; the constitutive equation is represented as follows:

$$T^m_m(t) = 3K(t)\Big(J(t) - J_N(t)\Big)$$

$$\frac{T'_{ij}(t)}{\mu(t)} = \frac{dr}{dt}\left[\left(B_{ij}(t) - \frac{I_B(t)}{3}\, g_{ij}\right) - \frac{T'_{ij}(t)}{G(t)}\right] \tag{76}$$

where t is the time, $t=0$ corresponds to the start of cure, the reference configuration corresponds to $t=0$ (it follows that $B_{ij}(0) = g_{ij}$, $J(0) = 1$), the time dependence of μ and G is defined implicitly via the time dependence of D-O-P, and

$$T'^{i}_{j}(t) = T^i_j(t) - \frac{T^m_m(t)}{3}\, g^i_j \tag{77}$$

and the corotational derivative of a second-order tensor (A_{ij}) is given by the following:

$$\frac{dr}{dt} A_{ij} = \frac{d}{dt} A_{ij} - \left(w^k_j A_{ki} + w^k_i A_{kj}\right) \tag{78}$$

where $\frac{d}{dt} A_{ij}$ is the material derivative and w^j_i is the spin tensor.

It's convenient to define a tensor $A_{ij}(t)$ which is a measure of the integrated viscous strain:

$$A_{ij}(t) \equiv B_{ij}(t) - \frac{I_B(t)}{3}\, g_{ij} - \frac{T'_{ij}(t)}{G(t)} \tag{79}$$

It follows Eq. (79) that A_{ij} is symmetric and $\mathrm{tr}\, A_{ij}(t) = 0$.

The constitutive equations may now be represented as follows:

$$T_m^E = 3K(t)\left(J(t) - J_N(t)\right)$$

$$\frac{T'_{ij}(t)}{\mu(t)} = \frac{d}{dt} A_{ij}(t) - \left[w_j^k(t)A_{ki}(t) + w_i^k A_{kj}(t)\right] \tag{80}$$

For the finite element technique the material derivatives must be expressed in terms of increments. The following representations are used:

$$\frac{d}{dt} A_{ij}(t_n) \simeq \frac{\Delta A_{ij}(t_n)}{\Delta t}$$

$$w_i^j(t_n) \simeq \frac{1}{2\Delta t}\left[\Delta F_i^K(t_n) F^{-1}{}_K^j(t_n) - \Delta F_K^j(t_n) F^{-1}{}_i^K(t_n)\right] \tag{81}$$

Eqs. (79), (80), and (81) complete the formulation of the constitutive equation. The global stiffness matrix required for the iterations is generated by Eq. (45).

The following idealized cure process is assumed in this study:

1) The component is cured for 2 hours at 350°F and a pressure of 85 psia. Time is measured from the start of the cure cycle, and the stresses throughout the compo nent are equivalent to the applied hydrostatic pressure at $t = 0$.

2) The environmental pressure is reduced to atmospheric pressure in the next 10 minutes and then the component is cooled to 75°F during the next 2 hours.

The following tabulation summarizes the material functions used for the numerical study, and it is assumed that they vary linearly with time between the instants given:

EPOXY

	TIME			
	0	2 hrs	2 hrs - 10 min	4 hrs - 10 min
$K(t)(10^6$ psi)	.16	.16	.16	.75
$G(t)(10^6$ psi)	.076	.076	.076	.18
$\mu(t)(10^4$ psi-min)	1.1	1.1×10^4	1.1×10^4	1.7×10^4
$J_N(t) - 1$	$.4375 \times 10^{-3}$	-.01757	-.01757	-.04017

PHENOLIC

	TIME			
	0	2 hrs	2 hrs - 10 min	4 hrs - 10 min
$K(t)(10^6$ psi)	.16	.16	.16	.75
$G(t)(10^6$ psi)	.076	.076	.076	.18
$\mu(t)(10^4$ psi-min)	1.1	1.1×10^4	1.1×10^4	1.7×10^4
$J_N(t) - 1$	$.4375 \times 10^{-3}$	-.17964	-.17964	-.2141

Some rationale for the values chosen is in order. Consider the epoxy characterization. Wang[15] published mechanical test data for cured epoxy. The values of K and G at 4 hrs - 10 min were selected to correspond to Wang's tensile test data at 72°F; the values of K and G at 2 hrs - 10 min and at 2 hrs were selected to correspond to his tensile test data at 375°F. The value of μ at 4 hrs - 10 min was selected to correspond to Wang's tensile creep data at 1000 psi and 375°F; the value of μ at 2 hrs - 10 min and 2 hrs was selected to correspond to his tensile creep data at 2000 psi and 73°F. The values of K, G, and μ at 0 hrs were

assumed with no experimental justification; the value of μ for the fluid-like uncured state of the material was chosen very small relative to its value for the cured state. Intuitively it appears that what happens during the cure cycle is less sensitive to K and G than to μ, and, since no data were available for these properties, the values of K and G were selected equal to their fully cured values. The value of J_N at 0 hrs was selected so that the stress in the resin corresponds to the applied hydrostatic pressure; the value of J_N at 2 hrs and 2 hrs - 10 min was selected to correspond to the polymerization dimensional change given by Table 3. The value of J_N at 4 hrs - 10 min was selected to correspond to the differential thermal expansion ($\Delta\varepsilon^T$) assuming graphite reinforcement given by Table 3.

Mechanical test data similar to Wang's for epoxy were not available for phenolic. The values of K,, G , and μ were selected to match those used for epoxy. The values of J_N were selected using the same rationale which was used for the epoxy.

The finite element model of the material is represented by Figure 14. Attention is concentrated on the resin surrounding a single fiber in a laminate of 50 volume %. It's assumed that the model represents a fiber in an interior lamina of a multi-directionally reinforced laminate. It's also assumed that the fibers are rigid relative to the resin (e.g., Young's modulus of a graphite fiber is 100 times that of epoxy). Advantages of symmetry are utilized by modeling only 1/4 of the fiber neighborhood. A thin plate of stiff (Hookian Elastic) material (represented by elements 1 through 6) is added to the top edge of the resin; it's used to apply and remove the controlled hydrostatic pressure and maintain flatness of the top edge. The circular boundary (contiguous with the fiber) is held fixed. On the other boundary the normal displacement and the shear traction are set to zero.

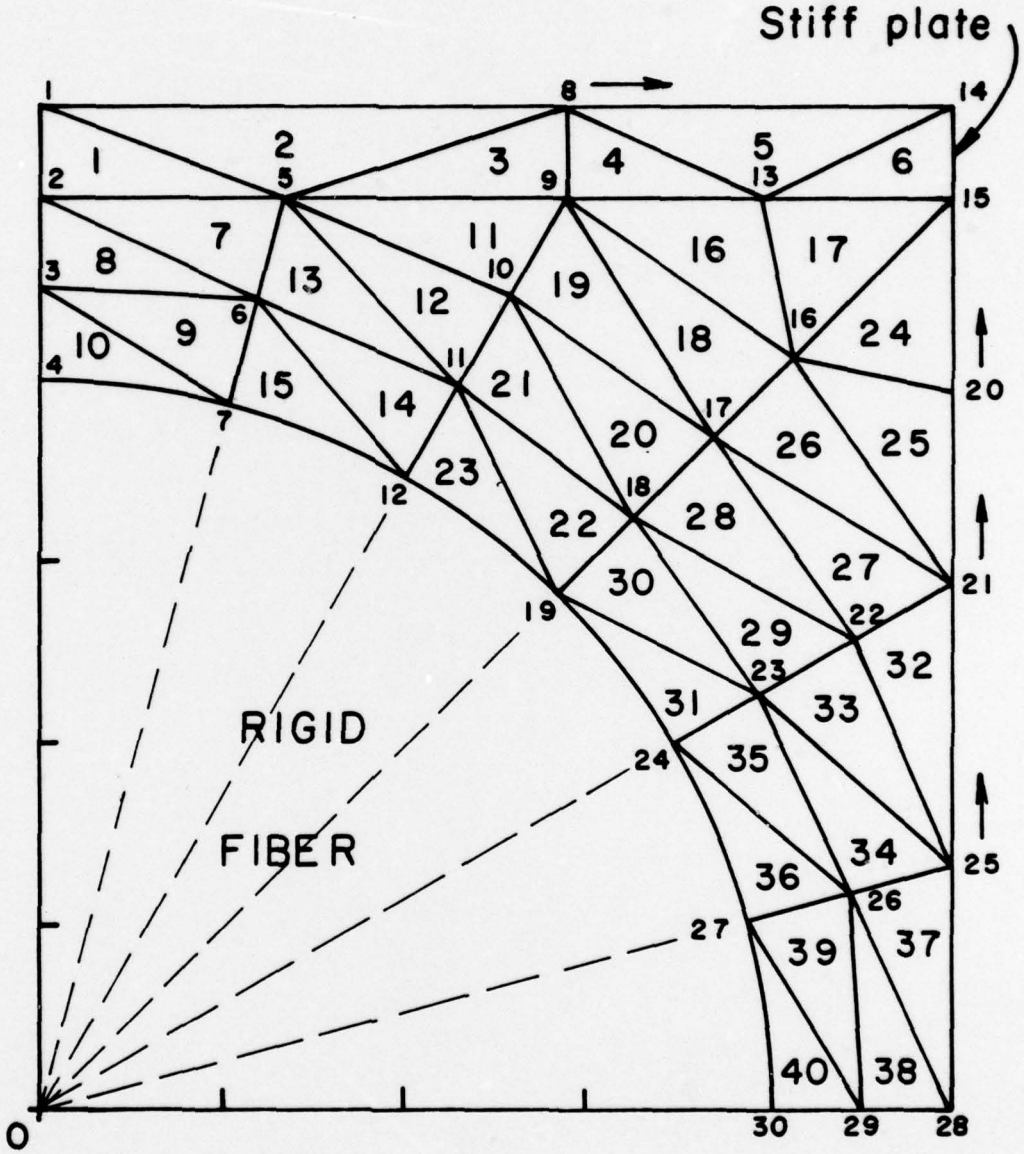

Figure 14. Finite element model.

The results are summarized by Figures 15 and 16. A review of the printout shows that the stresses are maximum generally in the neighborhood of Element #40 and that the state of stress is well represented by the mean stress (i.e., $T^m_m/3$) — because the deviatoric component is but a few percent of the mean stress. The cases were performed using an increment size of one minute and a convergence criterion of 1%.

The time history of the mean stress in Element #40 is presented for the epoxy resin by Figure 15 and for the phenolic resin by Figure 16. In order to present clearly the effects of polymerization dimensional change, two cases were studied for each resin; one case includes both polymerization and cool-down, and the second case includes only the cool-down. The results indicate a considerable effect on the residual stress — even for the epoxy resin.

The magnitude of the predicted stress is very large — approximately 50% greater than the reported uniaxial tensile strength of epoxy for the case without polymerization and the predicted stress is relatively greater for the other cases.

The numerical results presented by Figures 15 and 16 are the initial calculations performed. Obviously, the predicted values are sensitive particularly to the constitutive equations and the values of the material parameters used to represent the material behavior. More numerical studies and correlation with experimental data are required to establish the credibility and utility of the technology. Even so, one is tempted to derive conclusions from the numerical results even at this early time in the development of the technology. In that case it's unavoidable but to conconclude — for the composites studied — the following:

1) One may expect damage in the laminate — in the form of voids or cracks in the resin and/or debonding from the fiber — located between parallel fibers in a lamina.

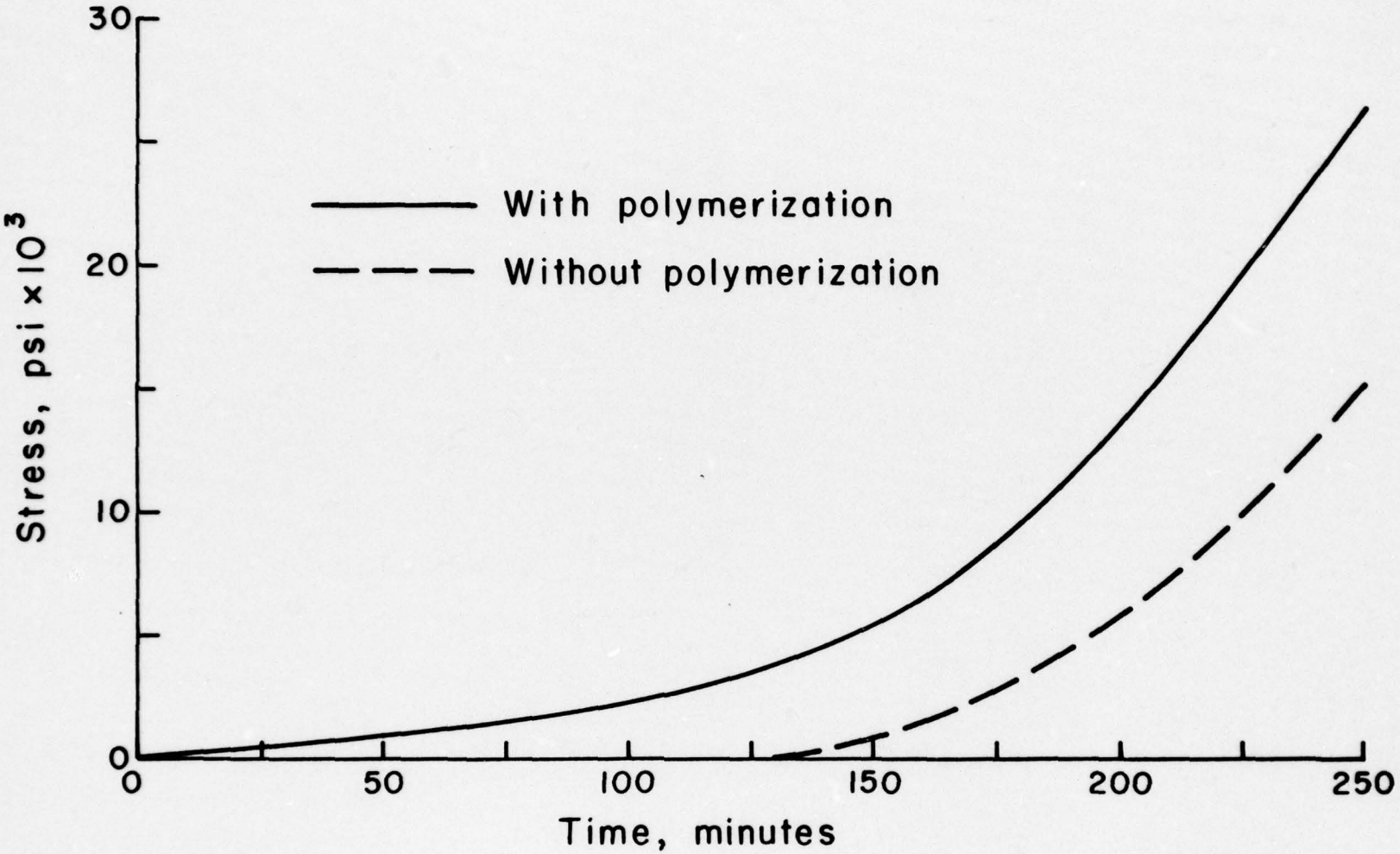

Figure 15. Mean stress in Element #40 for epoxy resin.

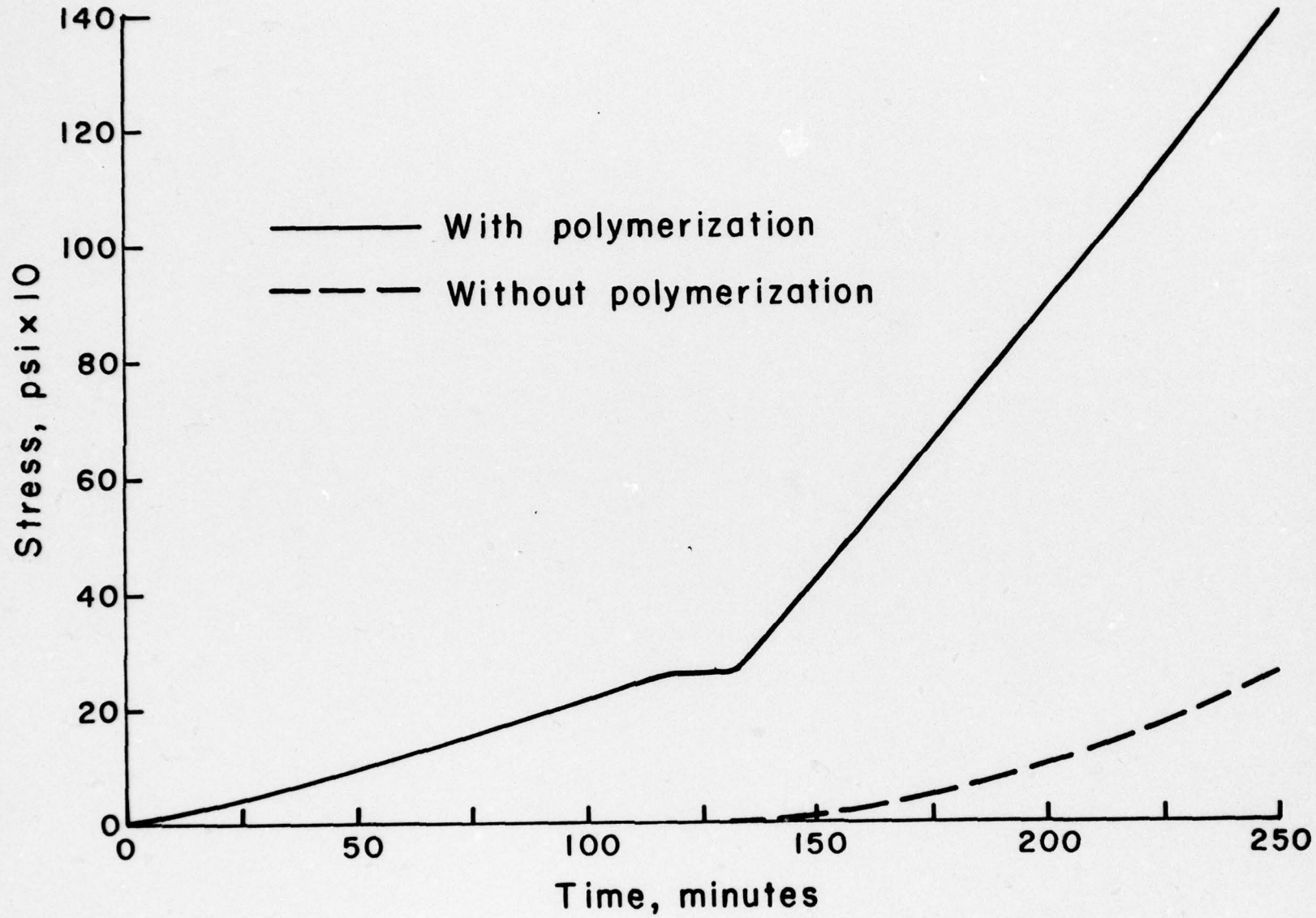

Figure 16. Mean stress in Element #40 for phenolic resin.

2) The dimensional changes associated with polymerization of the resin should not be neglected in the analysis of residual stress or damage resulting therefrom.

IV. REFERENCES

1. Truesdell, C. and Toupin, R.A., "Principles of Classical Mechanics and Field Theories," *Encyclopedia of Physics*, S. Flugge, Ed. (Springer-Verlag, Berlin, 1969), Vol. III, Pt 1.

2. Truesdell, C. and Noll, W., "The Nonlinear Field Theories of Mechanics," *Encyclopedia of Physics*, S. Flugge, Ed. (Springer-Verlag, Berlin, 1965), Vol. III, Pt. 3.

3. Stricklin, J.A., Haisler, W.E., and Von Riesemann, W.A., "Formulation, Computation, and Solution Procedures for Material and/or Geometric Nonlinear Structural Analysis by the Finite Element Method," Sandia Laboratories Contract Report SC-CR-72 3102, July 1972.

4. Oden, J.T., *Finite Elements of Nonlinear Continua*, McGraw-Hill, 1972.

5. Green, A.E. and Atkins, J.E., *Large Elastic Deformations*, Clarendon Press, Oxford, 2nd Ed., 1970.

6. Berg, C.A., "The Motion of Cracks in Plane Viscous Deformation," Fourth U.S. National Congress of Applied Mechanics, 1962.

7. Shaffer, B.W. and Levitsky, M., "Thermoelastic Constitutive Equations for Chemically Hardening Materials," J. of Applied Mechanics, September 1974.

8. Levitsky, M. and Shaffer, B.W., "Residual Thermal Stresses in a Solid Sphere Cast from a Thermosetting Material," J. of Applied Mechanics, September 1975.

9. Chamis, C.C., "Lamination Residual Stresses in Cross-Plied Fiber Composites," 26th Annual Technical Conference, 1971, Reinforced Plastics/Composites Division, The Society of the Plastics Industry, Inc.

10 Marloff, D., "Three-Dimensional Photoelastic Analysis of a Fiber-Reinforced Composite Model," Experimental Mechanics, April 1969.

11. Koufopoulos, T. "Shrinkage Stresses in Two-Phase Materials," J. Composite Materials, Vol. 3, April 1969.

12. Daniel, L. "Lamination Residual Stress in Fiber Composites," NASA CR-134826, March 1975, NASA CR-135085, June 1976.

13. Lee, B.L., Sacher, R.E., and Lewis, R.W., "Environmental Effects on the Mechanical Properties of Glass Fiber/Epoxy Resin Composites," AMMRC TR 77, Interim Report, May 1977.

14. Schwartz, E.B., and McQuillen, E.J., "Viscoelastic Creep and Relaxation in Laminated Composites," NADC-74196-30, 4 November 1974.

15. Wang, A.S.D., "Viscoelastic Creep Test of Epoxy Material," Drexel University, March 1973, Final Technical Report submitted to NADC, Warminster, PA.

SECURITY CLASSIFICATION OF THIS PAGE (When Data Entered)

REPORT DOCUMENTATION PAGE

READ INSTRUCTIONS BEFORE COMPLETING FORM

1. REPORT NUMBER: AFOSR-TR-78-0957	2. GOVT ACCESSION NO.
3. RECIPIENT'S CATALOG NUMBER	
4. TITLE (and Subtitle): A NEW FINITE ELEMENT TECHNIQUE AND A STUDY OF RESIDUAL STRESS IN COMPOSITE MATERIALS	5. TYPE OF REPORT & PERIOD COVERED: FINAL Rept. 15 Jun 76 - 30 Nov 77
	6. PERFORMING ORG. REPORT NUMBER: ARAP Report No 336
7. AUTHOR(s): THOMAS B. MCDONOUGH	8. CONTRACT OR GRANT NUMBER(s): F44620-76-C-0122 new
9. PERFORMING ORGANIZATION NAME AND ADDRESS: ARAP, INC 50 WASHINGTON RD PRINCETON, NJ 08540	10. PROGRAM ELEMENT, PROJECT, TASK AREA & WORK UNIT NUMBERS: 2307B1 61102F
11. CONTROLLING OFFICE NAME AND ADDRESS: AIR FORCE OFFICE OF SCIENTIFIC RESEARCH/NA BLDG 410 BOLLING AIR FORCE BASE, D C 20332	12. REPORT DATE: Apr 78 13. NUMBER OF PAGES: 66
14. MONITORING AGENCY NAME & ADDRESS (if different from Controlling Office): ARAP-336	15. SECURITY CLASS. (of this report): UNCLASSIFIED
12. 70 p.	15a. DECLASSIFICATION/DOWNGRADING SCHEDULE

16. DISTRIBUTION STATEMENT (of this Report)

Approved for public release; distribution unlimited.

17. DISTRIBUTION STATEMENT (of the abstract entered in Block 20, if different from Report)

18. SUPPLEMENTARY NOTES

19. KEY WORDS (Continue on reverse side if necessary and identify by block number)

FINITE ELEMENT	CREEPING FLOW
FINITE DEFORMATION	RESIDUAL STRESS
NONLINEAR	COMPOSITE MATERIAL
ITERATIVE SOLUTION	POLYMERIZATION PHASE
QUASI-STATIC DEFORMATION	COOL-DOWN

20. ABSTRACT (Continue on reverse side if necessary and identify by block number)

Two studies are presented in this report. The first is the development of a new finite element solution, and the second is an analysis of residual stress in filamentary composite material. The new feature of the finite element solution is in the formulation phase of the development; existing procedures are used for the numerical solution. The technique presented is restricted to problems usually described as quasistatic or creeping flow, but it is not restricted by small strain or rotation, nor is it specialized to a particular theory of constitutive behavior. Relative to existing codes the new technique may offer advantages for the study of solid-fluid interactions or for material behavior

DD FORM 1 JAN 73 1473 EDITION OF 1 NOV 65 IS OBSOLETE

008 400

UNCLASSIFIED

SECURITY CLASSIFICATION OF THIS PAGE (When Data Entered)

which fits neither of the concepts of solids or fluids. Four sample problems are studied. A comparison of numerical predictions with some exact analytic solutions is presented, and the comparison is excellent. The second study concerns residual stress. Its development in polymeric filamentary reinforced composite materials is discussed in terms of differential dimensional changes that occur during processing. Two phenomena which contribute to the development of residual stress are considered: dimensional change of the resin due to polymerization and differential thermal expansion of the resin and reinforcement upon cooling from the cure temperature to room temperature. Results of the study to date do not indicate that dimensional changes due to polymerization may be neglected in residual stress assessments.